

AD 655290

POSTIRRADIATION EXAMINATION OF THE
PM-3A TYPE 1 SERIAL 2 CORE
PART I. POSTIRRADIATION EXAMINATION
OF FUEL TUBES

to

UNITED STATES GOVERNMENT NAVY DEPARTMENT
FACILITIES ENGINEERING COMMAND
WASHINGTON, D. C. 20390

February 28, 1967

by

John B. Brown, Victor W. Storhok, and John E. Gates

Contract NBy-63910

Distribution of this
document is unlimited.

BATTELLE MEMORIAL INSTITUTE
Columbus Laboratories
505 King Avenue
Columbus, Ohio 43201

DDC
RECEIVED
JUL 28 1967
RECEIVED
B

RECEIVED

AUG 1 1967

CFSTI

Battelle Memorial Institute • COLUMBUS LABORATORIES

505 KING AVENUE COLUMBUS, OHIO 43201 • AREA CODE 614, TELEPHONE 299-3151 • CABLE ADDRESS: BATMIN

February 28, 1967

Commander J. C. LeDoux
United States Government Navy Department
Facilities Engineering Command
Washington, D. C. 20390

Dear Sir:

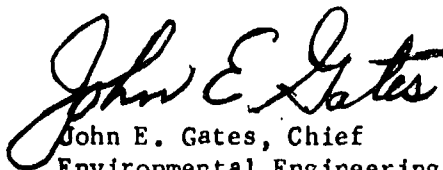
Contract NBy-63910

The program entitled "Postirradiation Examination of PM-3A Core", which Battelle-Columbus has been conducting for the Facilities Engineering Command, has been concluded. The final report describing the results of the examination has been completed in two volumes, and twenty copies of each volume are being provided for your use. Volume I describes examination of the core and fuel tubes. Examination of a control rod from the core is described in Volume II.

It has been a pleasure to conduct this program for the Navy and we hope that the results of this work will provide a greater understanding of the problems that arise in the operation of PM-type reactors.

If you have any questions concerning the two reports, please call me at Extension 2705, or John Brown at Extension 3283.

Very truly yours,


John E. Gates, Chief
Environmental Engineering Command

JEG/CD

Enclosure - 20 copies

Distribution of this
document is unlimited.

TABLE OF CONTENTS

	<u>Page</u>
ABSTRACT	1
INTRODUCTION	2
HISTORY	3
Pm-3A Fuel Core Specifications and Details of Fuel Element Construction	3
Specifications	3
Fuel Element Construction	5
Operational and Storage History	5
Irradiation History	5
Primary Water Chemistry	6
Demineralizer	9
Storage History	9
POSTIRRADIATION EXAMINATION	10
Experimental Procedures	10
Unloading and Inspection of Shipping Package	10
Hot-Cell Storage Pool	11
Core Bundle Unloading	11
In-Cell Core Bundle Handling	12
In-Cell Optical Aids	13
Stereoviewer	13
Borescope	13
Removal and Numbering of Fuel Tubes	13
Fuel Tube Diameter Measurements	14
Fuel Burnup Analysis	14
Fuel Tube Gamma Scan	16
Metallography	16
Analysis and Removal of Scale	17
Results	19
General Appearance of Core and Fuel Bundles	19
Visual Examinations of Fuel Tubes	22
Borescope Examination of Fuel Tubes	27
Fuel Tube Diameter Measurements	29
Fuel Burnup Analysis	29
Fuel Tube Gamma Scans	32
Metallography	35

TABLE OF CONTENTS (Continued)

	<u>Page</u>
As-Fabricated Fuel Tube	35
As-Irradiated Fuel Tubes	35
Void Fraction in UO_2 Particles	55
Chloride-Treated Fuel Tube	56
Scale Analysis	58
Physical Characteristics of Suspended Scale	58
Adherent-scale, X-Ray Diffraction Analysis	59
Suspended Scale, X-Ray Spectrographic Analysis	59
Nuclide Composition of Scale	59
Scale Color and Adherent Physical Characteristics	60
DISCUSSION	61
CONCLUSIONS	66
FUTURE WORK	67
REFERENCES	68, 69
ACKNOWLEDGMENT	70
APPENDIX A	A1-A12
APPENDIX B	B1

ABSTRACT

The PM-3A Type 1 Serial 2 core was prematurely discharged because of increasing fission product accumulation in the primary coolant system, presumably resulting from a fuel leak of undetermined origin. Fission product activity buildup was believed to be associated with defects in the 347 stainless steel cladding on the tubular-shaped fuel consisting of 28 v/o UO₂ dispersed in 304L stainless steel. The purpose of the fuel core examination was to locate fuel tube defects and to determine the cause(s) of such defects. Cracks were found to penetrate the outer cladding on high performance fuel tubes in regions where clad stresses and fuel burnup ($\approx 13 \times 10^{20}$ fissions/cm³) were at a maximum. All cracks detected were longitudinal in direction. Microstructural examination of the failure region showed clad cracks to be intergranular in nature, starting at the outside surface of the cladding and generally terminating at the surface of a UO₂ particle. Also, examination of stainless steel clad and fuel matrix microstructure showed no evidence of grain boundary precipitates or fuel matrix cracking. Crack morphology suggested the possibility of the cracking being aggravated by some type of corrosive attack that was activated by stress. On the strength of these limited observations and their similarity to defects attributed by other investigators to stress-activated corrosion, it was concluded that the most probable cause of clad cracking was a stress accelerated chemical attack of unknown origin.

INTRODUCTION

The PM-3A, Type 1 Serial 2, reactor core was ordered shut down November 13, 1964, after an accumulated lifetime of 7165 EFPH⁽¹⁾ (effective full power hours). This represented 52.8% of the core's design lifetime energy output (14.73 MW years). The core change was necessitated by an increasing fission product accumulation in the primary coolant system presumably resulting from a fuel leak of undetermined origin. At the time of reactor shutdown, the activity in the primary coolant had increased by a factor of approximately 1000⁽²⁾ since the leakage of fission products was first detected in June, 1964, after 4745 EFPH of plant operation.

The fission product activity buildup was believed to be associated with cracking of the stainless steel cladding on the stainless steel-UO₂ dispersion fuel tubes. In an attempt to locate the cracks and to determine the cause(s) of such cracking, the entire core was shipped to the Battelle-Columbus Hot Cells for examination. The details and results of the examination of the fuel tubes are presented in this report. Details and results of the examination of one control rod are presented in a separate volume of this report, Part II.

Work performed in the examination of the PM-3A core was sponsored by the Department of the Navy, Facilities Engineering Command. Core operation data was supplied by the United States Naval Nuclear Power Unit.

HISTORY

PM-3A Fuel Core Specifications and Details of Fuel Element Construction

Specifications

The PM-3A Core⁽³⁾ is a cylindrical heterogeneous, light-water-moderated, highly-enriched (93.1%) system which operates at a pressure of 1500 psia. The core consists of seven fuel bundles, six peripheral and one center bundle, contained in a core shroud. The total number of elements in the core is 849, with 139 in each peripheral bundle and 15 in the center bundle. Of this total number, 741 are tubular-type fuel elements having a characteristic 0.506-inch OD and 0.417-inch ID with a corresponding outside to total heat transfer area ratio of 0.548:1. The tubular fuel elements are 36 inches long with a 30-inch active length. The dispersion fuel core, clad with 0.007-inch 347 stainless steel inside and outside, is 0.030-inch thick with 28 v/o UO₂ dispersed in 3041 SS (U:93.3% U-235). The fuel elements and lumped poison rods are placed on a triangular pitch of 0.655 inches except across split lines. Figure 1 shows the top view of the complete core as it appeared in the opened shipping cask at Battelle-Columbus. Six Y-shaped control rods are used to control the reactivity of the core. Average operating core coolant temperature was 463 F, average clad surface temperature was 580 F, and maximum fuel matrix temperature was 620 F.



TE00213

FIGURE 1. TOP VIEW OF PM-3A TYPE 1 SERIAL 2 CORE
AS RECEIVED AT BATTELLE-COLUMBUS

Fuel Element Construction

The tubular fuel elements for PM-1 (Sundance) and PM-3A (McMurdo) were fabricated in approximately 80 basic operations from powder blending to finished fuel bundles. Major operations⁽⁴⁾ in the fabrication of the tubular fuel elements included blending of UO_2 and stainless steel powders and vertically rolling the powders into a green strip, sintering the strip, sheathing the strip in a thin (0.002-0.005-inch) clad to protect it from the atmosphere and hot-rolling it to 95-97 percent of theoretical density. End claddings were welded on and the composite formed into a tube which was fitted between inner and outer wrought cladding tubes. The assembly was then alternately drawn and annealed to size. For final densification and bonding, the tubes were hot isostatically pressed. Then the tubes were inspected and assembled into bundles.

Operational and Storage History

Irradiation History

The PM-3A power plant started operation in May, 1962, and was shut down November, 1964. The core accumulated 7165 effective full power hours of operation at a nominal power level of 9.5 MW(t). The average time integrated thermal neutron flux supported by the core was

about 2.6×10^{20} neutrons per square centimeter. Power distribution measurements⁽⁵⁾ on the cold-clean PM-3A reference design core showed the average integrated power in each fuel tube ranged in value from 0.87 to 1.56 times the core average power or a spread of a factor of 1.8 between the coolest and hottest tubes. It was also demonstrated that fuel tubes located in the center region of the core operated at the highest power levels which reached approximately 3.28 times the core average power. There was also some power peaking along the sides of the Y-rod channels and Y-rod guides.

Primary Water Chemistry⁽⁶⁾

Primary water radioactivity started to increase during the June, 1964, operating month and steadily increased until reactor shutdown in November, 1964. During the 1964 operating period the primary system chemistry control maintained all parameters within specifications, except for the demineralizer decontamination factor, activity levels, and dissolved oxygen and hydrogen⁽⁶⁾. The weekly average hydrogen was always within specifications. However, the minimum values reported for June, July, and August, 1964, were nearly always below the nominal operating minimum of 15 cc/l, but were never near the shutdown limit of 5 cc/kg. The use of ammonia to control the hydrogen and therefore oxygen concentration, as well as pH probably accounts for some of the variations observed.

The gross activity level in the coolant increased steadily from mid-June to late August, 1964, where it appeared to level off at about 10^{-1} $\mu\text{c/ml}$ as shown in Figure 2. ⁽⁷⁾ A decrease to about 4×10^{-2} $\mu\text{c/ml}$ was observed in September, but during October the activity again rose to a high of 4.5×10^{-1} $\mu\text{c/ml}$ before shutdown in November. During the periods of high activity the gross activity was characterized by a predominance of fission products, rather than the usual activation and corrosion products.

The gross iodine activity levels rose from 4×10^{-3} to 10^{-2} $\mu\text{c/ml}$ and appeared to level off in July. In August, however, the activity increased to 10^{-1} $\mu\text{c/ml}$ and again appeared to level off. The iodine activity level decreased during September to a low of 4.5×10^{-3} before climbing to about 2.5×10^{-1} $\mu\text{c/ml}$ in October. The decrease in gross iodine after shutdown in November was very slow indicating a considerable inventory of I-131 in the system. Only intermittent purification flow was used during the shutdown; as a consequence, the reduction in coolant activity was largely the result of radioactive decay, rather than removal by the demineralizer.

The reason for the decrease in activity in September, 1964, was not readily discernible but may have been due to obtaining a poor sample as a result of a partially plugged line. Site personnel reported release of some unidentified material from the sample line early in October. ⁽⁶⁾

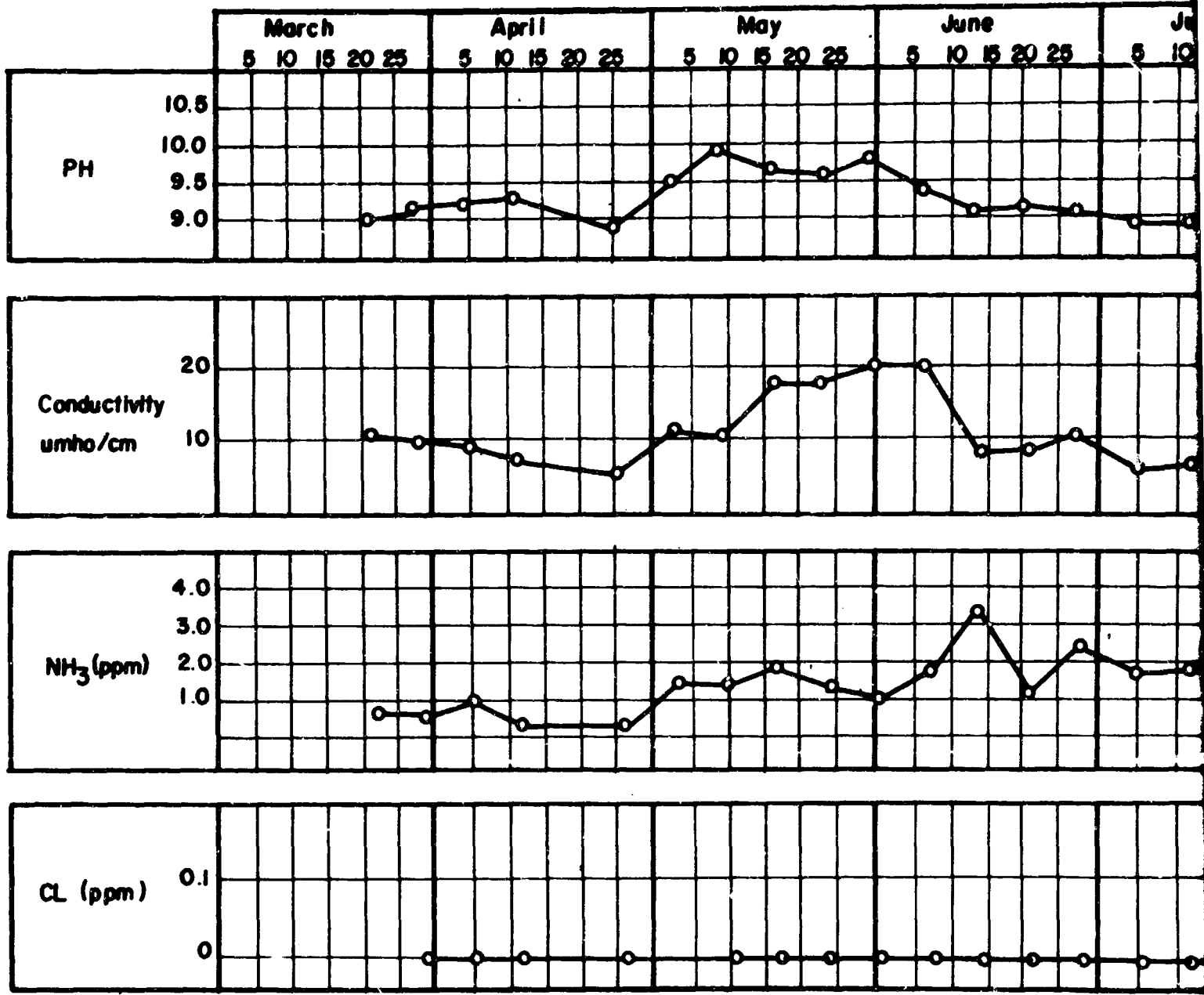
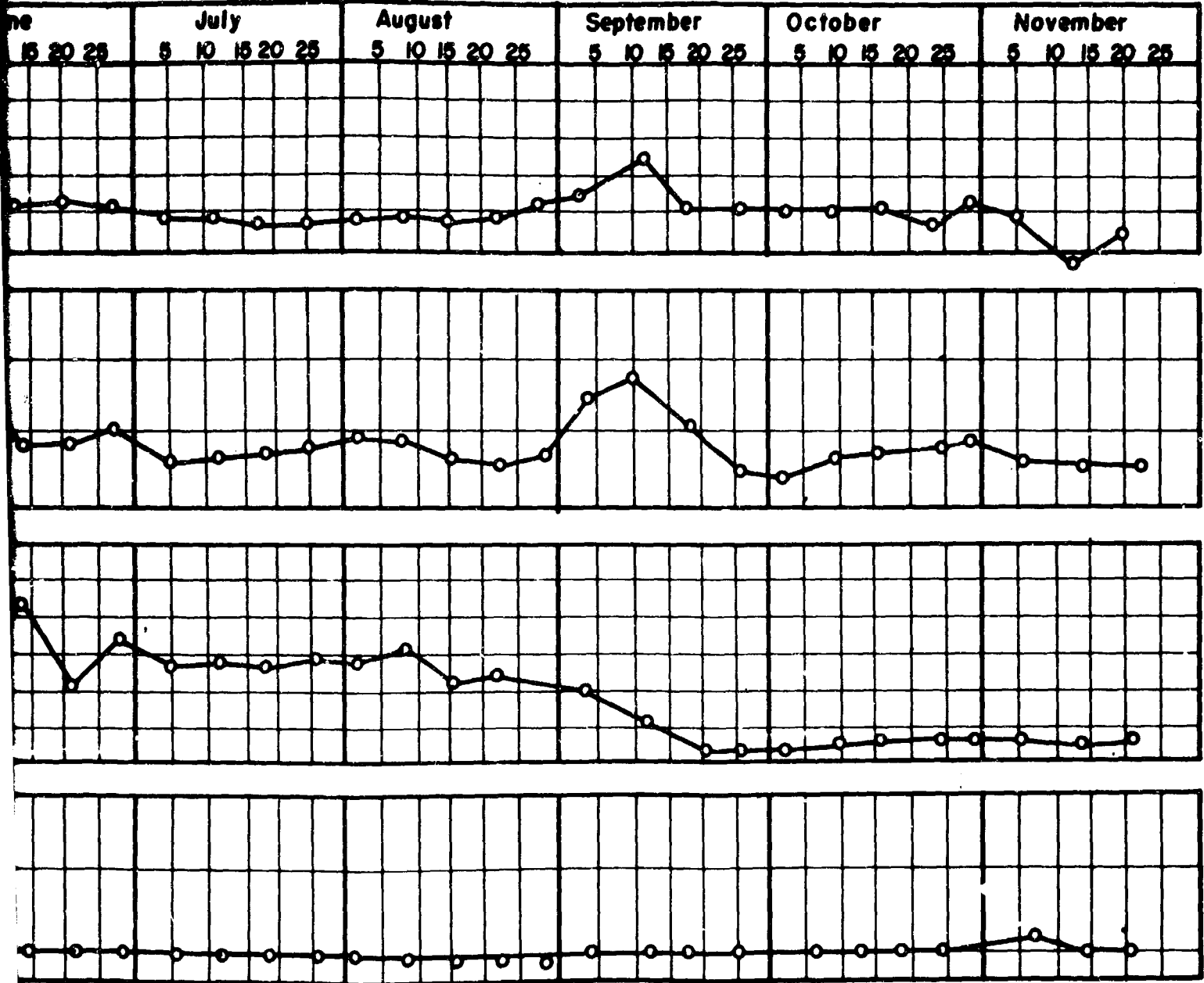


FIGURE 2a. PRIMARY COOLANT CHEMISTRY



PLANT CHEMISTRY

12

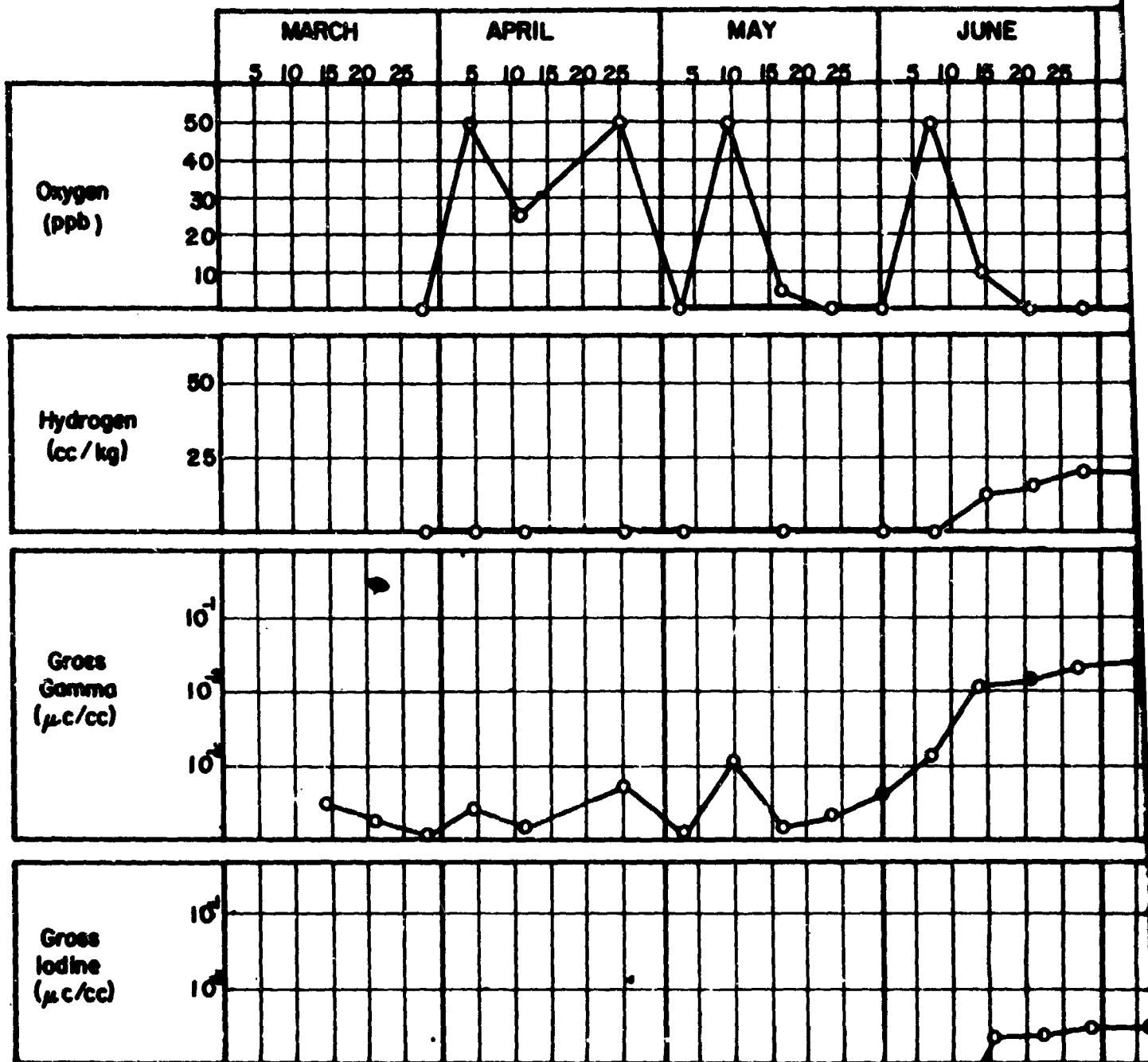
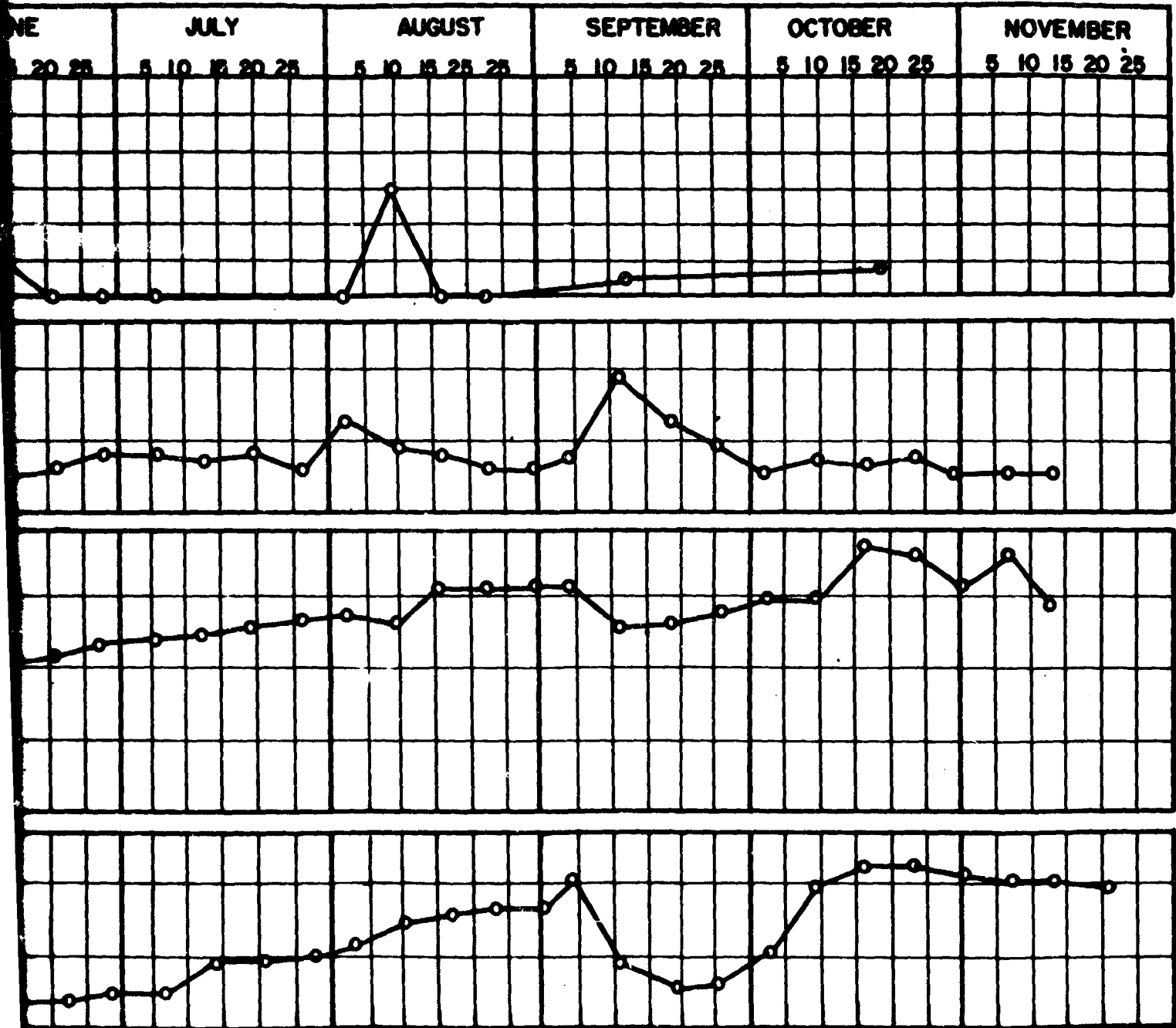


FIGURE 2b. PRIMARY COOLANT CHEM

A



LANT CHEMISTRY

B

Demineralizer (6)

A mixed-bed ion exchange demineralizer was provided for the primary coolant system to maintain the purity of the water and to prevent excessive buildup of radioactivity. Since an ammonia-based resin was one of the components, a basic pH was maintained as long as there was an exchange of cations with ammonium ions. The ion exchange resins removed radioactive elements from the water, either by true ion exchange or by physical retention. The latter was the mechanism by which the bulk of insoluble corrosion products (crud) was removed from the water.

Storage History

The PM-3A reactor was refueled in December, 1964. The spent core was transferred from the pressure vessel tank to the storage tank where the core was placed in the PM-3A shipping cask. Upon unloading the PM-3A core and shipping cask from the storage pool, methanol was added to the cask coolant water to prevent freezing. Due to the gas pressure buildup, the methanol was later flushed out of the cask with demineralized water. Radioactive cesium and cobalt-58 were detected in samples of the methanol-water solution that was flushed from the cask. The core was stored on-site until the spring of 1966, when it was shipped to the Battelle-Columbus Hot Cell Facility for examination to determine the cause(s) of activity buildup.

POSTIRRADIATION EXAMINATION

The postirradiation examination of the PM-3A core was directed toward identification of the cause(s) of fission product leakage from the PM-3A fuel tubes. A combination of visual macroexamination for defects followed by metallographic or microstructural examination of apparent defect areas was utilized in the examination. These were supplemented with dimensional measurements, fuel burnup analysis, gamma scanning and analysis of the corrosion products. The experimental procedures used in the examination and the results are described in the following sections.

Experimental Procedures

Unloading and Inspection of Shipping Package

The PM-3A shipping package was received, inspected, and dismantled in the following manner:

- (1) The PM-3A shipping package was shipped from Davisville, Rhode Island, to Battelle-Columbus Laboratories via Long Island Nuclear Service Corporation, and arrived at the Columbus Laboratories the afternoon of April 7, 1966. The as-received package was then off-loaded from the shipping vehicle and transferred to the Hot Cell dock area.

- (2) The shipping package and associated hardware were inspected for any damage. No damage was found, Appendix A.
- (3) Temperature measurements were performed on cask fins and body at several cask locations before and after cask shroud plate was removed, Appendix A.
- (4) Locked compartments (two) were opened; cask gas pressure was noted and cask gas and water samples were taken, Appendix A.
- (5) Remaining pieces of hardware were removed from the shipping package and cask was readied for submersion in the Hot Cell storage pool.

Hot-Cell Storage Pool

The PM-3A shipping cask was unloaded and stored in a 14-foot-deep by 6-foot-wide by 12-foot-long water-filled storage pool. Softened well water was used to fill the pool. Chemical analysis of the softened water showed the chloride concentration to be 6.1 ppm.

Core Bundle Unloading

The shipping cask lid was removed after placing the cask on the bottom of the 14-foot-deep storage pool. Sixty cadmium rods were

added to the core as a precautionary measure against criticality contingencies. Using the appropriate core handling tools, the core handling fixture (Appendix B) was removed and the center bundle and peripheral bundles No. 9 and 12 were carefully pulled from the core. A 0-400 pound scale was placed between a one-ton hand hoist and the bundle handling tools, and the hand hoist was in turn connected to a one-ton electric motor-driven hoist. The center bundle was pulled with no forces exceeding 100 pounds as registered on the scale, and the peripheral bundles were pulled with forces not exceeding 250 pounds. Each time a bundle was removed from the core, visibility would be momentarily obstructed by a small burst of black scale. Fuel bundles were then transferred to the beta-gamma cell via a lead transfer cask. Only one fuel bundle was removed from the core at one time and examined in the cell. Shielding during the fuel bundle transfers from the pool-to-Hot Cell and back again from the Hot Cell-to-pool was provided by a 5-inch-thick lead transfer cask with overall dimensions compatible to in-cell handling. The transfer cask remained full of water during the transfers and during bundle storage within the high-level cell.

In-Cell Core Bundle Handling

Care was exercised during all in-cell handling of the core bundles to prevent any bumping or scraping of the bundle surfaces on foreign cell hardware. By utilizing the beta-gamma cell crane, a special

shortened peripheral bundle handling tool, a cable-suspended bundle-carrying tray, and remotely-operated manipulator arms, it was possible to place the peripheral or center bundles at any desired location within the cell.

In-Cell Optical Aids

Stereoviewer. Nondestructive in-cell macroexaminations of the fuel bundles were performed at magnifications up to 12 diameters using a remotely-operated stereoviewer.

Borescope. Macroexaminations of the inner cladding tubes of the fuel tubes were conducted using a Lenox Instrument Company borescope with circumference viewing head. The borescope was capable of penetrating 36 inches into a 0.25-inch ID tube. Object magnification through the borescope was 1X.

Removal and Numbering of Fuel Tubes

Fuel tubes were cut from fuel bundles 12 and C using a remotely operated motor tool driving a 1/8-inch-thick Norton dry cutoff wheel. Fuel tubes scheduled for removal were chosen partly as a result of the macroexaminations and partly as an attempt to obtain low, medium, and high-performance fuel tubes for further examination. Both peripheral bundles 9 and 12 (the only peripheral bundles examined) exhibited crack indications

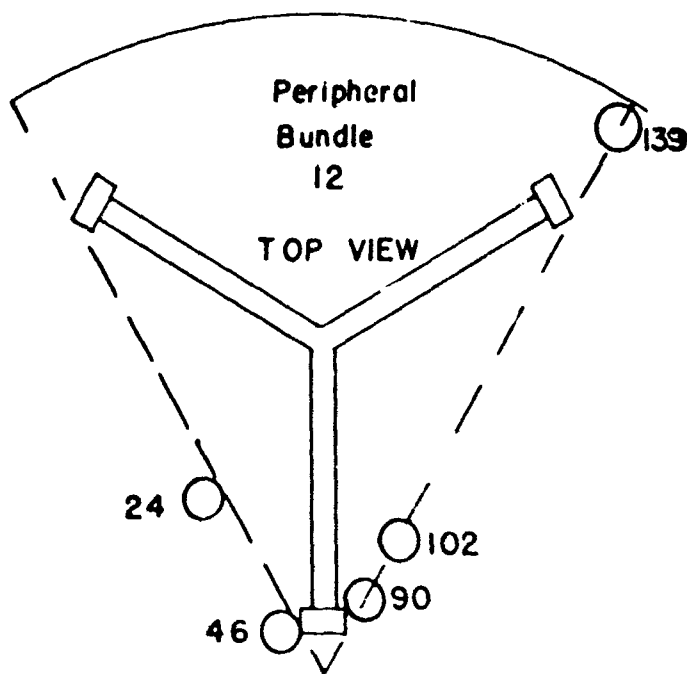
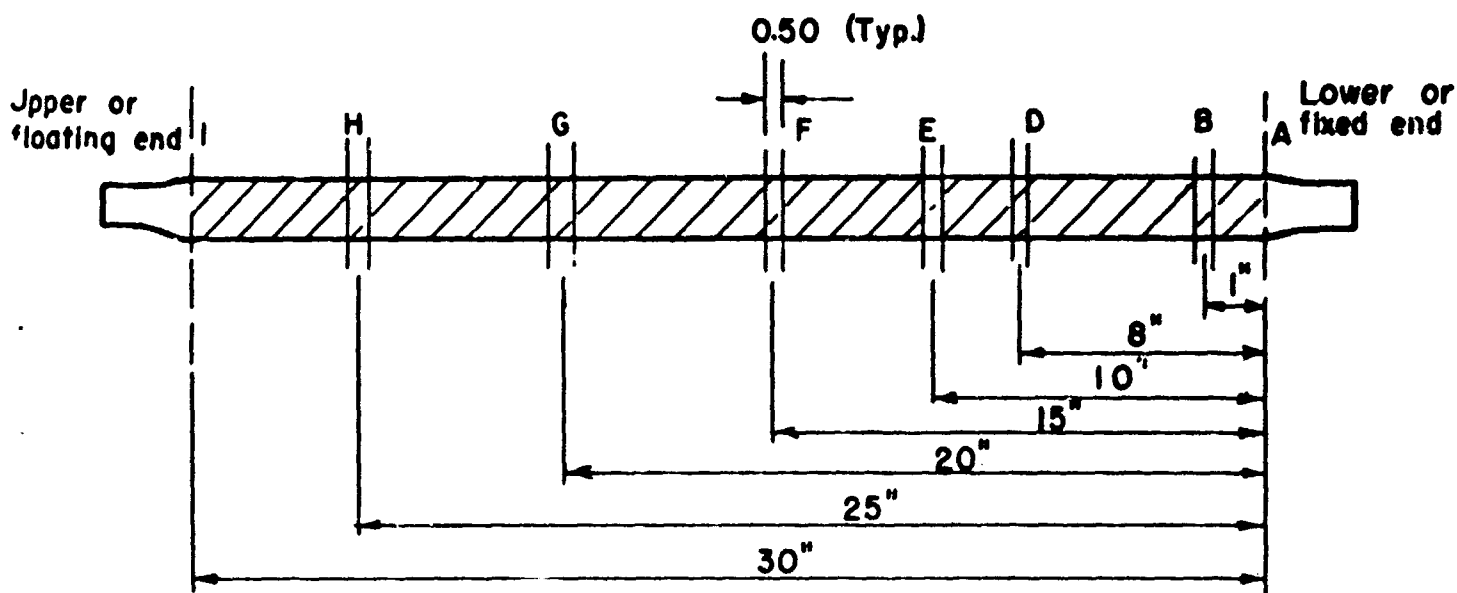
on high-performance fuel tubes. Bundle 12 was chosen for destructive examination only as a convenience, as it was present in the cell at the time of decision to proceed with fuel tube removal operations. Bundle C, the center bundle, was chosen because it contained highest performance fuel tubes. Fuel tubes cut from the bundles were numbered and placed in marked conduit tubing for reference. Tubes were identified by two numbers: the first number designated the bundle number (i.e., the Type 1, Serial 2 core bundles were numbered 7, 8, 9, 10, 11, 12, and C) and the second number designated the location within the particular bundle. The examined fuel tubes within peripheral bundle 12 were arbitrarily numbered as shown in Figure 3. No numbering scheme was used to identify the fuel tubes within the center bundle as the two fuel tubes removed from this bundle were taken from equivalent symmetry locations within the bundle.

Fuel Tube Diameter Measurements

Fuel tube diameter measurements were made using a vernier micrometer accurate to within ± 0.0005 inch. Diameter measurements were performed on six of the seven fuel tubes cut from the fuel bundles.

Fuel Burnup Analysis

Uranium burnup analyses were performed on two specimens taken from a high-performance fuel tube. One specimen was taken from a high-performance region of the fuel tube, and the other specimen was taken from



Fuel Tube Number

- 12-46
- 12-46
- 12-46
- 12-46
- 12-46
- 12-46
- 12-45
- 12-46
- 12-90
- 12-102
- 12-139
- 12-C
- 12-C

Metallography Specimen Number

- 12-46-A
- 12-46-B
- 12-46-D
- 12-46-E
- 12-46-F
- 12-46-G
- 12-46-H
- 12-46-I
- 12-90-E
- 12-102-E
- 12-139-E
- 12-C-1-E
- 12-C-2-E

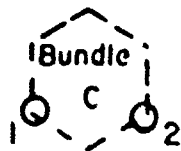


FIGURE 3. SCHEDULE OF WHEEL CUTS IN THE FUEL TUBES FOR METALLOGRAPHY

a low-performance region of the fuel tube. Each specimen was a cylindrical section of the fuel tube about 1/8-in. long. The specimens were dissolved and aliquots were analyzed by mass spectrographic techniques. The quantity of U^{234} , U^{235} , U^{236} , U^{238} was determined and compared to similar data from an unirradiated control specimen. The burnup was then calculated from the relationship:

$$BU = 100 \left[\frac{(1 + \alpha)(E_5^0 - E_5)}{E_5^0(1 + \alpha - E_5)} \right]$$

where

BU = w/o U-235

E_5^0 = initial enrichment, U-235,

E_5 = final enrichment, U-235,

α = 0.185.

Fuel Tube Gamma Scans

Three fuel tubes were gamma scanned to obtain profiles of the gamma radiation emitted from high performance, average performance, and low performance tubes. By correlating the gamma activity plots with chemical burnup analytical data, the burnup profile along the tube length was determined.

Metallography

Fourteen metallographic specimens were cut from six fuel tubes. Four of the fuel tubes were taken from peripheral bundle No. 12 and the remaining two fuel tubes were taken from the center bundle. The metallographic

specimens were cut from the several fuel tubes using a motor-driven 1/16-inch-thick abrasive blade. Figure 3 shows the schedule of abrasive wheel cuts used in the sectioning of the six fuel tubes. No attempt was made to preserve rotational orientation of the fuel tubes with respect to the tubes' longitudinal axis.

Metallographic sections were selected as a result of macroexamination of the fuel tubes. Wheel cuts were made to intersect the surface direction of crack indications at right angles, i.e., transverse sections were made for longitudinal crack indications. No transverse crack indications were detected. Two longitudinal metallographic sections were made to represent the postirradiated condition of the fuel dispersion-dead end interface at both ends of a typical high-performance fuel element.

Polished specimen surfaces were obtained by (1) grinding through 600-grit silicon carbide paper, (2) rough polishing with Linde A powder mixed with 2% Cr_2O_3 in water, and (3) fine polishing with Linde A and B powder with water as a carrier. The specimens were etched with a reagent containing glycerine, nitric acid, and hydrochloric acid.

Analysis and Removal of Scale

A black scale found adhering to the fuel tubes and suspended in the shipping cask coolant was analyzed to establish its identity, using radiochemical and X-ray diffraction techniques. Attempts were made to remove the adherent scale on two fuel tubes, using two different aqueous

solutions. The first solution to be tried consisted of 20 grams sulfamic acid dissolved in 20 ml of deionized water. The second solution consisted of the following:

	<u>Quantity</u>
Concentrated hydrochloric acid	90 ml
Ethylene glycol	90 ml
Borax	15 gm
Zinc chloride	15 gm
Ammonium fluoride	15 gm
H ₂ O	90 ml

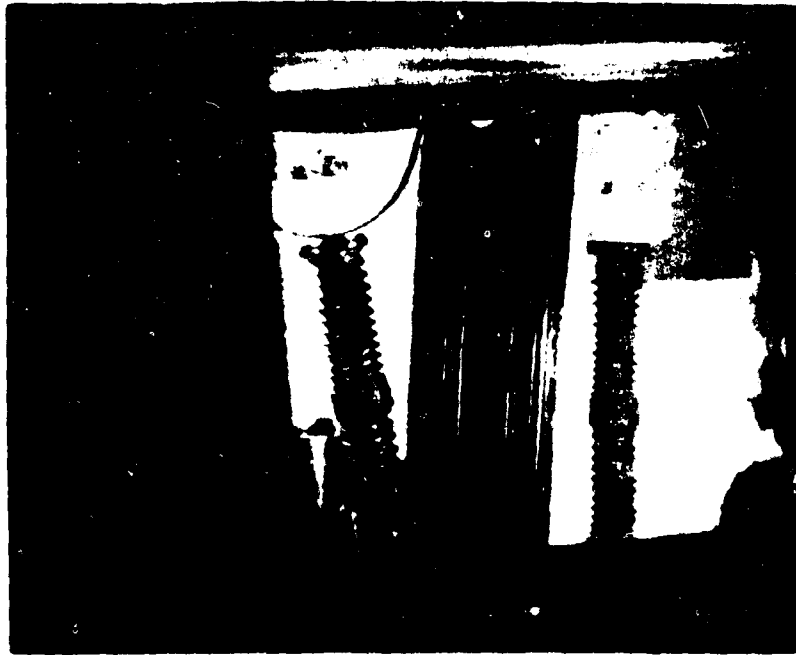
Fuel tubes No. 12-24 and 12-139 were immersed in the boiling sulfamic acid solution for up to ten minutes. The tubes were then visually inspected. Since this treatment did not remove the scale, the fuel tubes were immersed in the second boiling solution for up to ten minutes, followed by visual inspection. The second solution was used partly as an attempt to remove the scale by using a stronger solution and partly to determine whether clad stresses in a low-performance tube were sufficient to activate chloride attack to the clad.

Results

General Appearance of Core and Fuel Bundles

As the lid was removed from the shipping cask, a cloud of black particles was discharged into the pool from within the cask. The cloud eventually dispersed and was removed via pool filters. After a 24-hour period, particulate matter from the pool water trapped in the filter emitted gamma radiation resulting in a 200 MR/hr radiation field at the outside surface of the filter canister. Gamma ray spectrometer analysis showed the active nuclides to be Fe-59, Co-58, Mn-54, Co-60, and Y-91. The top view of the spent core after removal of the cask lid and core handling fixture was shown earlier in Figure 1. Black scale was observed coating the surface of the six peripheral bundles and center bundle. The shiny rings which appear on the top of several peripheral bundles were a consequence of the chafing action between the peripheral bundle hold-down screws and the peripheral bundle top grid plates.

Figure 4 shows peripheral bundle 9 after being lifted from the transfer cask within the beta-gamma cell. Figure 5 shows the control rod exit end of the peripheral bundle 9. Several of the cadmium rods, placed in the core as an added precaution against criticality, are visible in Figure 5. Figure 6 shows end views (less control rod) of peripheral bundle 12. As shown in the above photographs, all core bundle exterior surfaces were coated with a black scale. Passage of light through the tubes provided evidence that the scale buildup did not block any of the coolant flow



TE00216



TE00215

b.

FIGURE 4. PERIPHERAL BUNDLE AS IT APPEARED THROUGH THE HOT-CELL WINDOW



TE00222

FIGURE 5. CONTROL-ROD EXIT-END VIEW OF
PERIPHERAL BUNDLE 9

passages, Figure 6. The shiny areas on the fuel tubes shown in Figure 4a correspond to high-performance regions where most of the scale had flaked off.

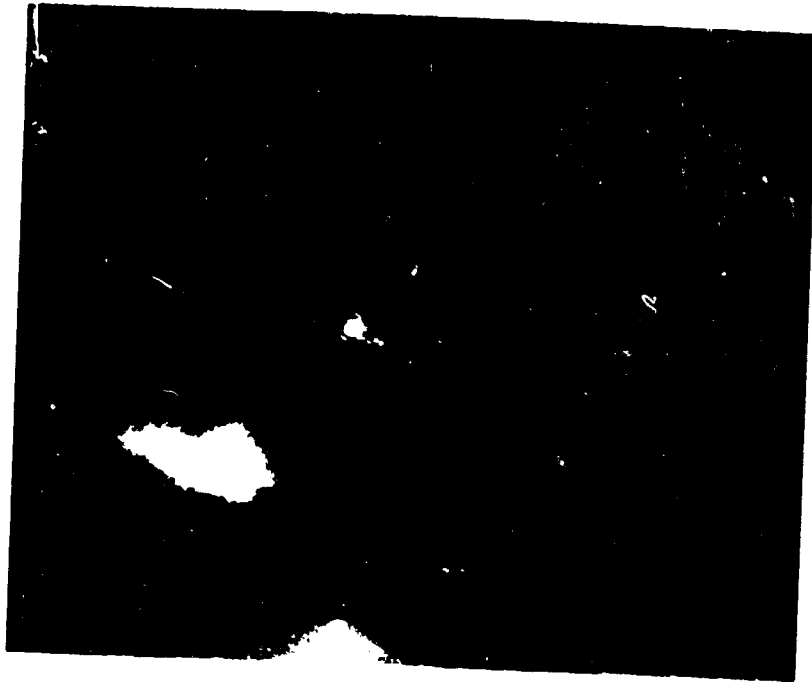
Figure 7 shows a photograph of the center bundle as it appeared through the cell window. Again the thick outer scale had flaked off in the high-performance domain of the bundle.

It was observed that the center bundle appeared to be twisted. Each time a peripheral bundle was removed from the core or placed back into the core, the center bundle had to be removed. This added attention to the center bundle may have produced the twisting.

Visual Examinations of Fuel Tubes

Examination of tube outer surfaces at 6X and 12X magnifications revealed the presence of numerous longitudinal cracks on several tubes. Figure 8 shows typical photomicrographs of crack indications and crud formation. Figure 8a is a 12X micrograph of several crack indications detected on fuel tube 12-46, i.e., bundle 12, tube 46. All crack indications were located in the high-performance domain of fuel tubes toward the center of the core. There appeared to be a crud buildup in the region adjacent to the cracks. Crack indications on fuel tube 46, bundle 9 are shown in Figure 8b.

Figure 9 shows a 6X photomicrograph composite of crack indications as they appeared on a high-performance region of fuel tube 12-46. Microstructural analysis of a specimen cut from this region of fuel tube 12-46 indicated that the darker cigar-shaped spots depicted in the composite outlined intergranular cracks.



a. Upper End

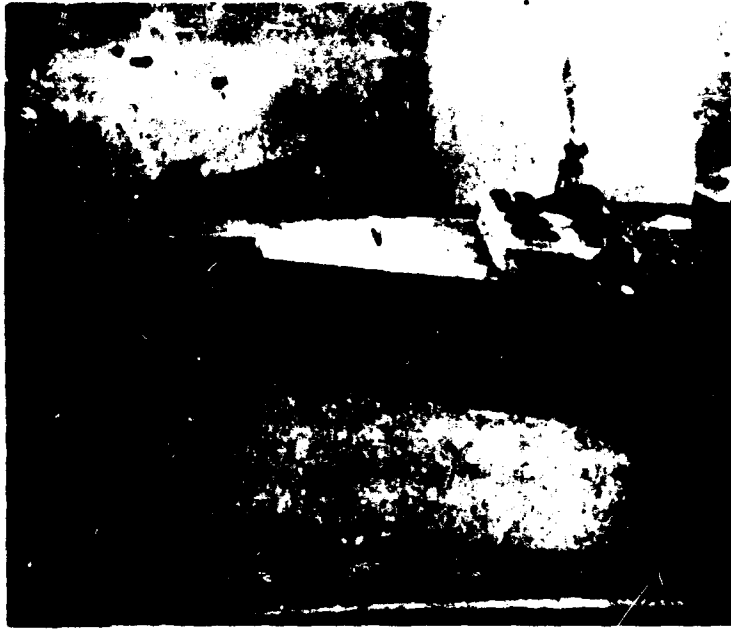
TE00340



b. Lower End

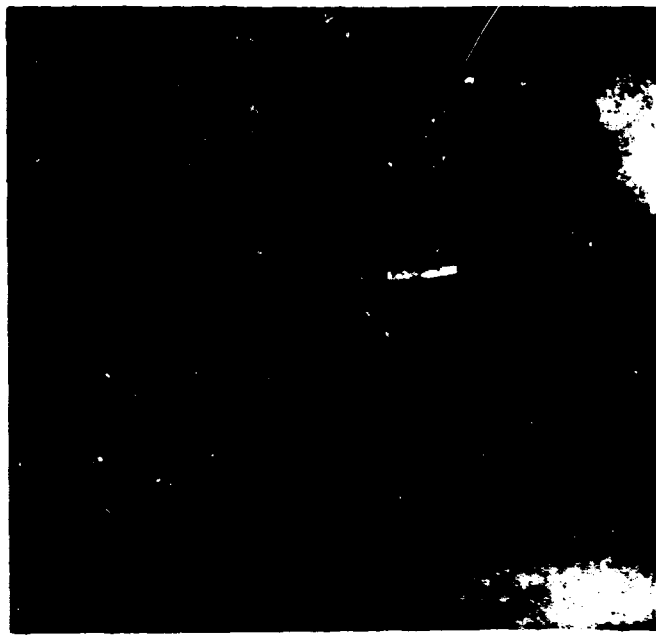
TE00349

FIGURE 6. END VIEWS OF PERIPHERAL BUNDLE 12,
LESS CONTROL ROD



TE00352

a.



TE00345

b.

FIGURE 7. CENTER BUNDLE AS IT APPEARED THROUGH THE CELL WINDOW



12X a. Fuel Tube 12-46 HC18507



12X b. Fuel Tube 9-46 HC18500



12X c. Fuel Tube 9-30 HC18495

FIGURE 8. REPRESENTATIVE CRACK INDICATIONS AND SCALE FORMATION ON PERIPHERAL-BUNDLE FUEL TUBES



P116 to P119

6X

FIGURE 9. PHOTOMICROGRAPH COMPOSITE OF HIGH-PERFORMANCE REGION OF FUEL TUBE 12-46

Figure 10 shows typical crack indications and scale formation on center bundle fuel tubes. Crack indications located in a high-performance domain of a center bundle fuel tube are shown in Figure 10a. The appearance of scale in low performance domains of center bundle fuel tubes is shown in Figure 10b, -c, and -d.

In general, the appearance of the fuel tube surfaces where the scale had flaked off was characterized by a dull metallic luster. All crack indications detected in the high-performance regions of the fuel tubes where the scale had flaked off were longitudinal in direction which implies that hoop-stresses may have been a significant factor in the failure mechanism. No blisters were noted on the fuel tubes which were examined. Tooling marks (longitudinal and spiraling circumferential) evidently incorporated into the cladding during fuel tube fabrication, were observed on some of the tubes. At least one crack appeared to be associated with a tooling mark, Figure 10a. While probably not the primary cause of failure in the fuel tubes such marks can act as stress raisers which could lead to premature failure of otherwise sound tubes.

Borescope Examination of Fuel Tubes

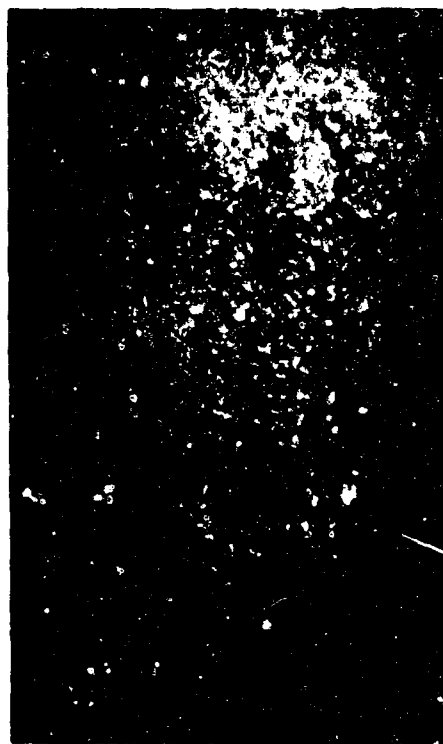
No indications of cracking of the inside cladding were observed during borescope examination of the fuel tubes in the two peripheral bundles which were inspected. With the exception of the surfaces located in high-performance regions of the fuel bundles, the inner clad surfaces were covered



6X a. Crack Indication, High- Performance Domain P242



6X b. Scale Formation, Low- Performance Domain P238



6X c. Scale Formation, Low- Performance Domain P230



6X d. Scale Formation, Low- Performance Domain P239

FIGURE 10. REPRESENTATIVE CRACK INDICATIONS AND SCALE FORMATION ON CENTER-BUNDLE FUEL TUBES

with a black oxide scale. The absence of cracking on the inner clad surface implied that inner clad stresses were not of the same mode and/or magnitude as the outer clad stresses.

Fuel Tube Diameter Measurements

In an attempt to determine relative swelling behavior along fuel tube lengths, the outer diameters of six fuel tubes were measured at every inch of fuel length. The results of these measurements are tabulated in Table 1. Diameters of fuel tube 12-46 are plotted as a function of longitudinal position along the tube in Figure 11. No attempt was made to descale the fuel tubes before the diameters were measured and some scatter was introduced to the data because of the nonuniform scale on the tube surfaces. As mentioned previously, the black scale had flaked off the high-performance regions of the fuel tubes. Average measured diameters ranged from 0.506 (close to nominal as-fabricated diameter) at a position 10 in. from the top of the fuel to 0.509 in. at a position 22 in. from the top of the fuel. The trend toward larger diameters in the high-performance region is shown in Figure 11. The regions of large diameter also corresponded to defected regions suggesting that cracking of the clad was related to strain.

Fuel Burnup Analysis

The burnup of two fuel specimens taken from a high-performance fuel tube (C-2) located in the center bundle was determined by mass spectrometric

TABLE 1. DATA FOR FUEL TUBE DIAMETER MEASUREMENT

Distance From Top, in.	Fuel Tube 12-46			Fuel Tube 12-90			Fuel Tube 12-102			
	0°	90°	Ave.	0°	90°	Ave.	0°	90°	Ave.	
1	0.5087	0.5090	0.5089	0.5080	0.5074	0.5077	0.5058	0.5096	0.5072	0.
2	0.5086	0.5082	0.5084	0.5086	0.5087	0.5087	0.5074	0.5098	0.5086	0.
3	0.5089	0.5083	0.5086	0.5083	0.5068	0.5076	0.5087	0.5087	0.5087	0.
4	0.5092	0.5086	0.5089	0.5070	0.5069	0.5070	0.5086	0.5080	0.5080	0.
5	0.5091	0.5090	0.5091	0.5071	0.5071	0.5071	0.5090	0.5086	0.5088	0.
6	0.5090	0.5085	0.5088	0.5076	0.5075	0.5076	0.5090	0.5077	0.5084	0.
7	0.5093	0.5093	0.5093	0.5078	0.5080	0.5079	0.5082	0.5066	0.5074	0.
8	0.5078	0.5112	0.5095	0.5075	0.5086	0.5081	0.5072	0.5068	0.5070	0.
9	0.5072	0.5069	0.5071	0.5075	0.5088	0.5082	0.5070	0.5068	0.5069	0.
10	0.5070	0.5070	0.5070	0.5077	0.5080	0.5079	0.5070	0.5072	0.5071	0.
11	0.5074	0.5072	0.5073	0.5074	0.5076	0.5075	0.5072	0.5073	0.5073	0.
12	0.5073	0.5070	0.5072	0.5074	0.5078	0.5076	0.5078	0.5074	0.5076	0.
13	0.5077	0.5076	0.5077	0.5080	0.5083	0.5082	0.5080	0.5072	0.5076	0.
14	0.5078	0.5072	0.5075	0.5081	0.5082	0.5082	0.5081	0.5085	0.5083	0.
15	0.5082	0.5077	0.5080	0.5086	0.5083	0.5085	0.5085	0.5083	0.5084	0.
16	0.5081	0.5076	0.5079	0.5088	0.5088	0.5088	0.5086	0.5078	0.5082	0.
17	0.5074	0.5080	0.5077	0.5089	0.5087	0.5088	0.5084	0.5079	0.5082	0.
18	0.5075	0.5075	0.5075	0.5089	0.5088	0.5089	0.5088	0.5078	0.5083	0.
19	0.5078	0.5082	0.5080	0.5090	0.5090	0.5090	0.5088	0.5088	0.5088	0.
20	0.5082	0.5089	0.5086	0.5092	0.5091	0.5092	0.5087	0.5091	0.5089	0.
21	0.5080	0.5088	0.5084	0.5091	0.5089	0.5090	0.5089	0.5088	0.5089	0.
22	0.5081	0.5098	0.5089	0.5087	0.5091	0.5089	0.5088	0.5088	0.5088	0.
23	0.5088	0.5099	0.5089	0.5087	0.5090	0.5089	0.5088	0.5090	0.5089	0.
24	0.5087	0.5104	0.5096	0.5093	0.5093	0.5093	0.5087	0.5092	0.5090	0.
25	0.5070	0.5067	0.5079	0.5090	0.5091	0.5091	0.5090	0.5088	0.5089	0.
26	0.5069	0.5068	0.5069	0.5089	0.5088	0.5089	0.5080	0.5086	0.5083	0.
27	0.5068	0.5070	0.5069	0.5089	0.5089	0.5089	0.5077	0.5089	0.5083	0.
28	--	--	--	0.5087	0.5089	0.5088	0.5081	0.5091	0.5086	0.
29	--	--	--	0.5085	0.5083	0.5084	0.5080	0.5085	0.5083	0.
30	--	--	--	0.5086	0.5064	0.5065	0.5068	0.5065	0.5067	0.

1. DATA FOR FUEL TUBE DIAMETER MEASUREMENTS

Tube 12-90		Fuel Tube 12-102			Fuel Tube 12-139			Fuel Tube C-2		
90°	Ave.	0°	90°	Ave.	0°	90°	Ave.	0°	90°	Ave.
0.5074	0.5077	0.5058	0.5096	0.5072	0.5045	0.5052	0.5049	0.5076	0.5069	0.5073
0.5087	0.5087	0.5074	0.5098	0.5086	0.5073	0.5076	0.5075	0.5077	0.5070	0.5074
0.5068	0.5076	0.5087	0.5087	0.5087	0.5076	0.5074	0.5075	0.5070	0.5065	0.5068
0.5069	0.5070	0.5088	0.5080	0.5080	0.5082	0.5072	0.5077	0.5066	0.5063	0.5065
0.5071	0.5071	0.5090	0.5086	0.5088	0.5071	0.5074	0.5073	0.5065	0.5064	0.5065
0.5075	0.5076	0.5090	0.5077	0.5084	0.5075	0.5073	0.5074	0.5064	0.5063	0.5064
0.5080	0.5079	0.5082	0.5066	0.5074	0.5072	0.5083	0.5078	0.5069	0.5065	0.5067
0.5086	0.5081	0.5072	0.5068	0.5070	0.5078	0.5076	0.5077	0.5068	0.5065	0.5067
0.5088	0.5082	0.5070	0.5068	0.5069	0.5079	0.5078	0.5079	0.5070	0.5068	0.5069
0.5080	0.5079	0.5070	0.5072	0.5071	0.5079	0.5076	0.5078	0.5069	0.5068	0.5069
0.5076	0.5075	0.5072	0.5073	0.5073	0.5082	0.5082	0.5082	0.5069	0.5070	0.5070
0.5078	0.5076	0.5078	0.5074	0.5076	0.5084	0.5089	0.5087	0.5069	0.5070	0.5070
0.5083	0.5082	0.5080	0.5072	0.5076	0.5088	0.5082	0.5085	0.5068	0.5069	0.5069
0.5082	0.5082	0.5081	0.5085	0.5083	0.5080	0.5080	0.5080	0.5071	0.5073	0.5072
0.5083	0.5085	0.5085	0.5083	0.5084	0.5086	0.5080	0.5083	0.5073	0.5077	0.5075
0.5088	0.5088	0.5086	0.5078	0.5082	0.5089	0.5080	0.5085	0.5080	0.5082	0.5081
0.5087	0.5088	0.5084	0.5079	0.5082	0.5083	0.5078	0.5081	0.5084	0.5093	0.5089
0.5088	0.5089	0.5088	0.5078	0.5083	0.5081	0.5081	0.5081	0.5088	0.5090	0.5089
0.5090	0.5090	0.5088	0.5088	0.5088	0.5088	0.5082	0.5085	0.5088	0.5089	0.5089
0.5091	0.5092	0.5087	0.5091	0.5089	0.5096	0.5082	0.5089	0.5093	0.5087	0.5090
0.5089	0.5090	0.5089	0.5088	0.5089	0.5089	0.5088	0.5089	0.5106	0.5079	0.5093
0.5091	0.5089	0.5088	0.5088	0.5088	0.5094	0.5091	0.5093	0.5103	0.5078	0.5091
0.5090	0.5089	0.5088	0.5090	0.5089	0.5093	0.5090	0.5092	0.5098	0.5083	0.5091
0.5093	0.5093	0.5087	0.5092	0.5090	0.5084	0.5089	0.5087	0.5089	0.5080	0.5085
0.5091	0.5091	0.5090	0.5088	0.5089	0.5087	0.5089	0.5088	0.5088	0.5080	0.5084
0.5088	0.5089	0.5080	0.5086	0.5083	0.5076	0.5090	0.5083	0.5091	0.5078	0.5085
0.5089	0.5089	0.5077	0.5089	0.5083	0.5078	0.5084	0.5081	0.5086	0.5077	0.5082
0.5089	0.5088	0.5081	0.5091	0.5086	0.5077	0.5078	0.5078	0.5080	0.5077	0.5079
0.5083	0.5084	0.5080	0.5085	0.5083	0.5074	0.5072	0.5073	0.5074	0.5073	0.5074
0.5064	0.5065	0.5068	0.5065	0.5067	0.5062	0.5068	0.5065	0.5070	0.5071	0.5071

30

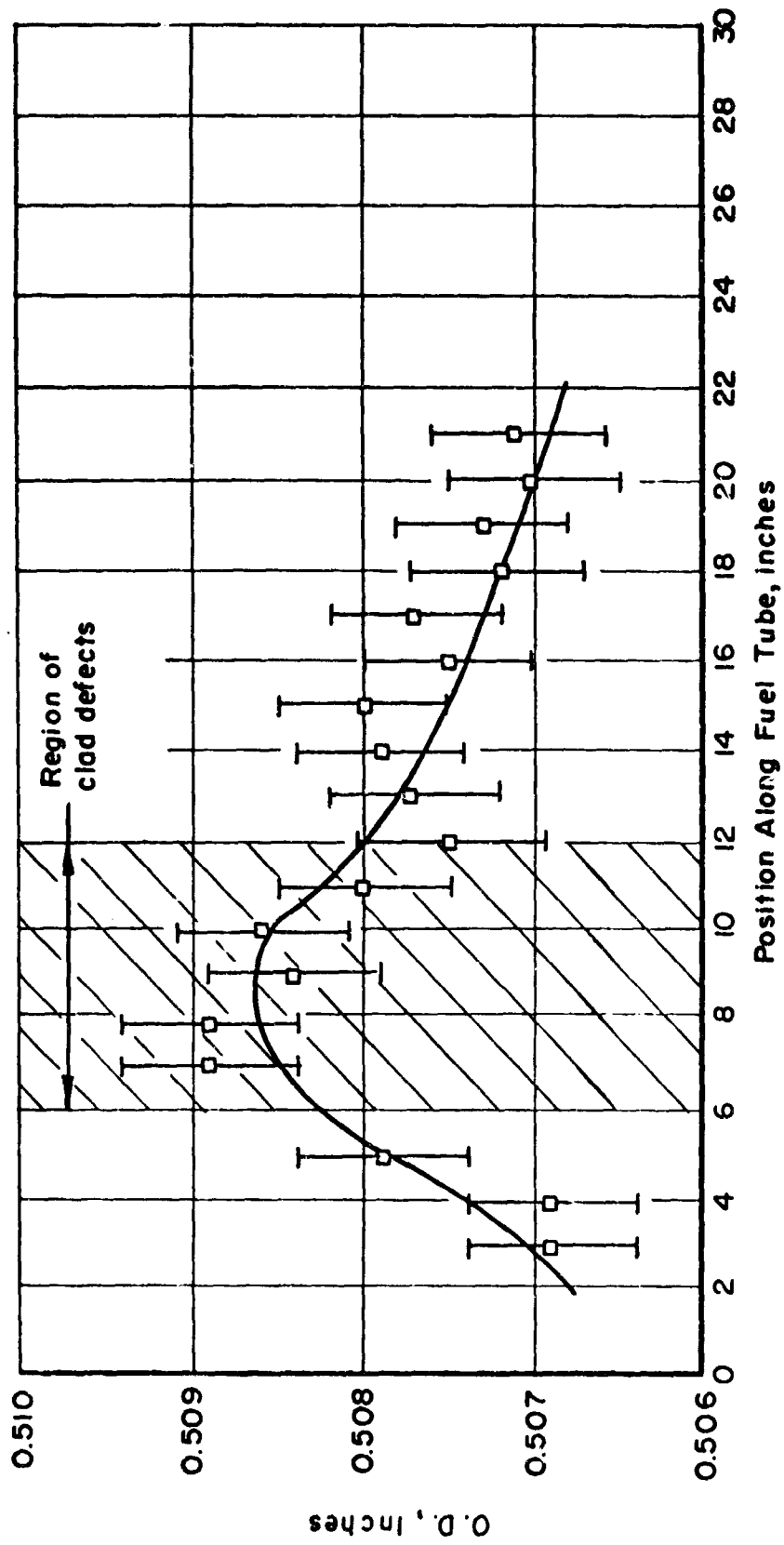


FIGURE 11. AVERAGE O.D. FOR FUEL TUBE 12-46

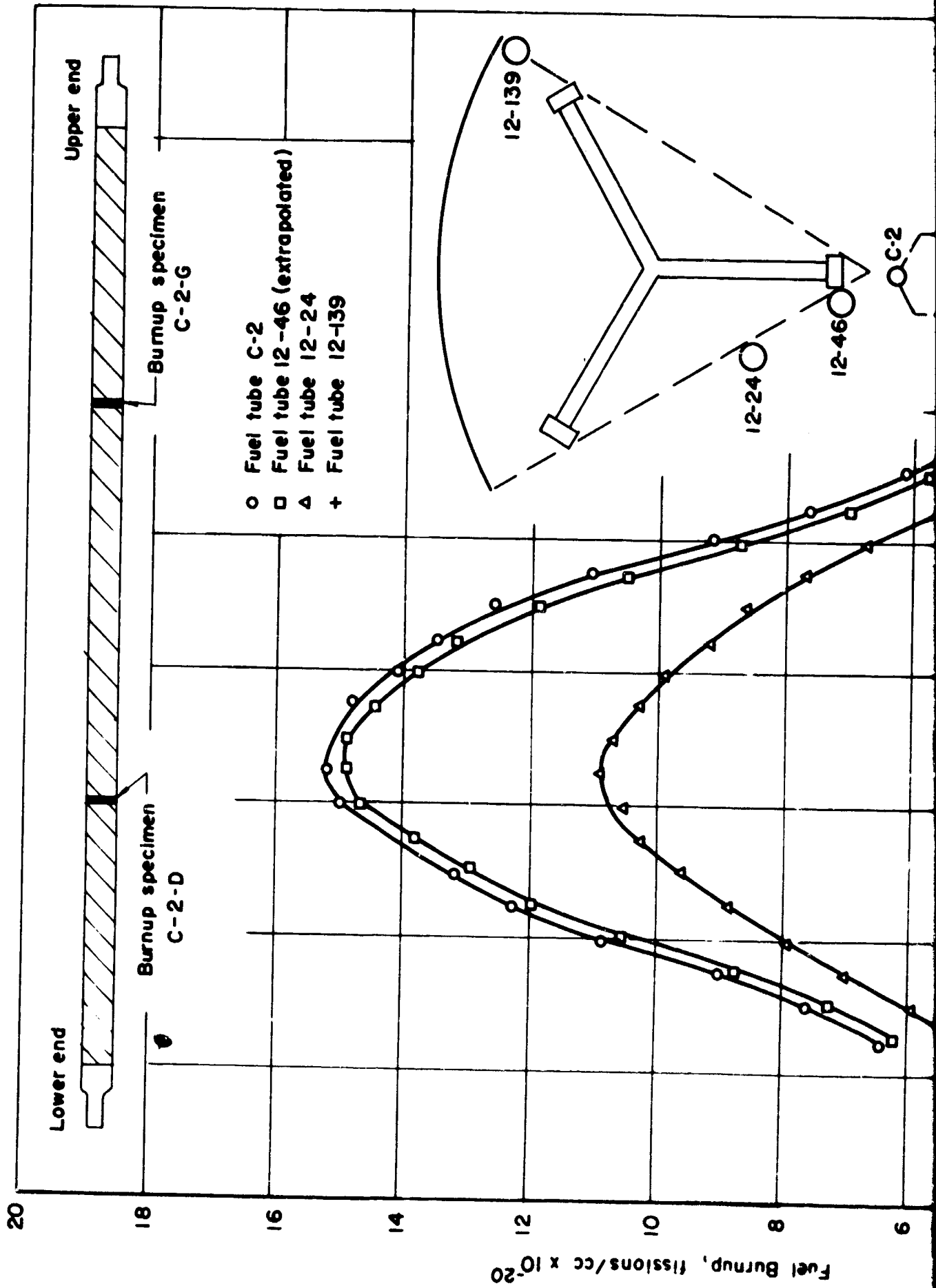
analysis for uranium isotopes. The two specimens were taken from the D and G positions of the fuel tube as defined in Figure 3. Table 2 gives the results of the burnup analysis. These burnup data were used to calibrate the fuel element gamma scan profiles presented in the next section.

Fuel Tube Gamma Scans

Fuel tubes No. 139 and 24 were cut from bundle 12 and fuel tube C-2 was cut from the center bundle. The fuel tubes were gamma scanned to determine fission product ($\text{Nb}_{95}\text{-Zr}_{95}$) concentration along the longitudinal direction of the fuel tubes. The fuel tubes were selected to represent low, medium, and high burnups. The burnup profile of the fuel tube was then estimated by correlating the analyzed fuel burnup at a given location with the measured gamma intensity at that location, and converting the gamma intensity data to fuel burnup. Figure 12 shows the gamma count rate calibrated in units of U-235 fissions/cc as a function of longitudinal position along the fuel tube. As shown in Figure 12, the peak burnups for all three fuel tubes appear to lie between 9 and 10 in. from the bottom end of the active core. The peak burnups experienced by the fuel were on the order of 15×10^{20} fissions/cc. This burnup occurred in a region centered approximately 10 in. from the bottom of the core with a radial expanse including the center bundle fuel tubes and an annulus concentric and adjacent with the center bundle containing several fuel tubes from each peripheral bundle.

TABLE 2. BURNUP OF FUEL TUBE NO. C-2

Specimen	Isotopic Content, w/o				Burnup, Fissions/cc	Position of Specimen From Bottom of Core, in.
	U-234	U-235	U-236	U-238		
Control C-10	1.03	93.18	0.26	5.53	0	--
C-2-D	1.17	84.80	7.02	7.01	15×10^{20}	8
C-2-G	1.06	91.30	1.79	5.85	4.2×10^{20}	20



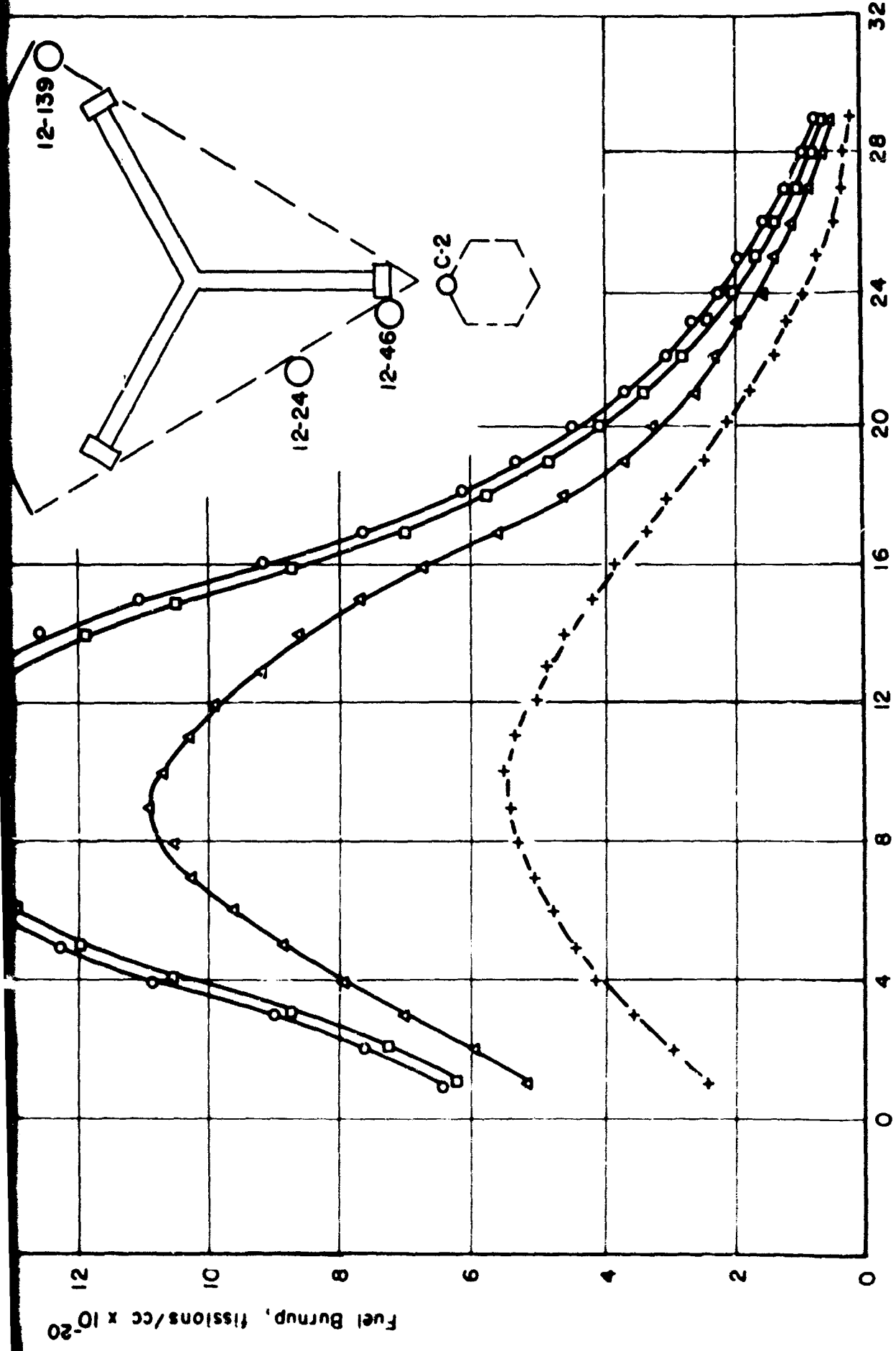


FIGURE 12. FUEL TUBE BURNUP AS A FUNCTION OF LONGITUDINAL POSITION

Burnup profile data shown in Figure 12 for fuel tube 12-46 were obtained by interpolation of burnup profile data from neighboring fuel tubes C-2 and 12-24, since fuel tube 12-46 was not gamma scanned before it was sectioned.

Metallography

The microstructure of fuel tubes before and after irradiation, and after irradiation followed by treatment in a chloride solution was studied by metallographic techniques. The results of the metallographic examination are summarized in Table 3. Details of the metallographic examination are discussed in the following sections.

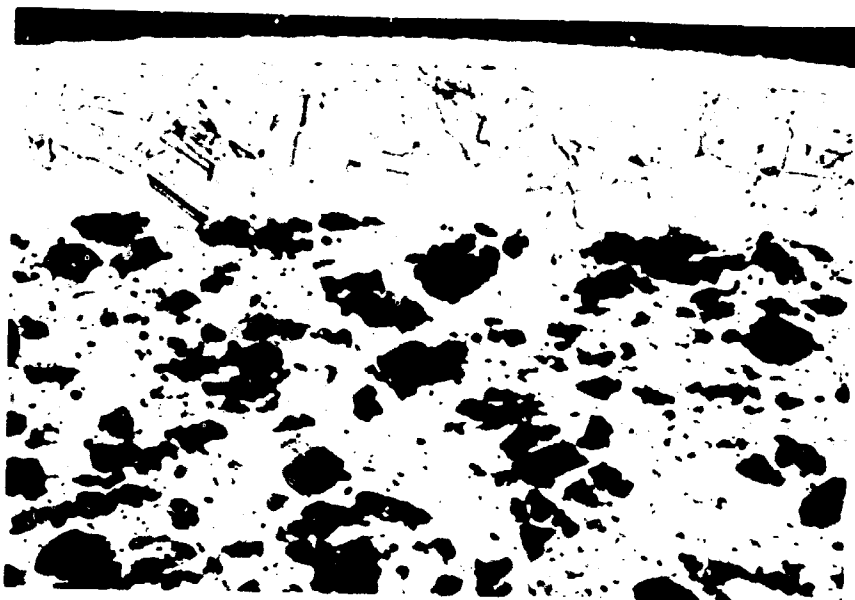
As-Fabricated Fuel Tube. Micrographs depicting the microstructure of an as-fabricated PM-3A fuel tube are shown in Figure 13. Examination of the microstructure indicated that the fuel dispersion was metallurgically bonded to the cladding. It was noted that the grain size and orientation was such that from 3 to 6 grains spanned the clad thickness (about 7 mils).

As-Irradiated Fuel Tubes. A schedule of metallographic specimens cut from the as-irradiated fuel tubes was shown in Figure 3. The high performance fuel tube, No. 12-46, was most extensively sectioned for

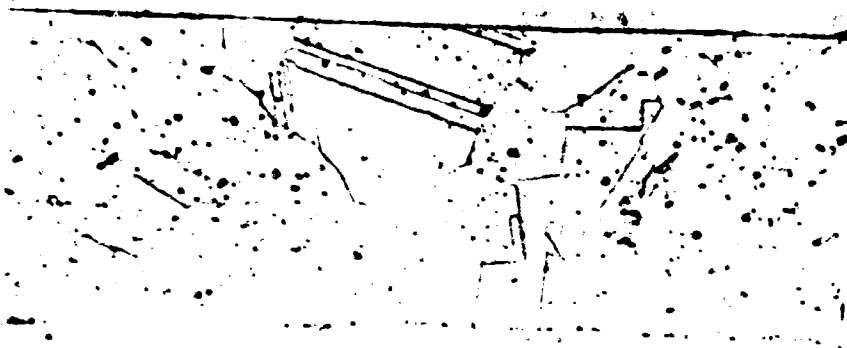
TABLE 3. RESULTS OF METALLOGRAPHIC EXAMINATION OF FUEL TUBES FROM PM-3A
TYPE 1 SERIAL 2 CORE

Metallography Specimen No.	Estimated Burnup, (fissions/cc) 10 ²⁰	Porosity in Fuel Particles, v/o	Fuel Tube O.D. at Specimen (a) Location	Remarks
12-46-A	6.0	--	0.507	No cracks in clad.
12-46-B	6.5	16	0.507	Ditto
12-46-D	14.6	24	0.509	Numerous intergranular cracks in outer clad terminating at fuel particles.
12-46-E	14.8	26	0.509	Ditto
12-46-F	7.6	18	0.508	One intergranular crack ter- minating midway through outer clad.
12-46-G	4.1	--	0.507	No cracks in clad.
12-46-H	1.7	--	0.507	Ditto
12-46-I	0.5	--	0.507	Ditto
12-90-E	14.0	--	0.509	Few intergranular outer cracks terminating in outer clad.
17-102-E	10.0	20	0.50 ^r	No cracks in clad
C-1-E	15.1	35	--	Very many intergranular cracks in outer clad terminating at fuel particles.
C-2-E	15.1	38	0.509	Ditto

(a) Measurements in low performance regions of the fuel tubes include scale adhering to surface.



a.
100X
Etched
24148



b.
250X
Etched
24156



c.
500X
Etched
24159

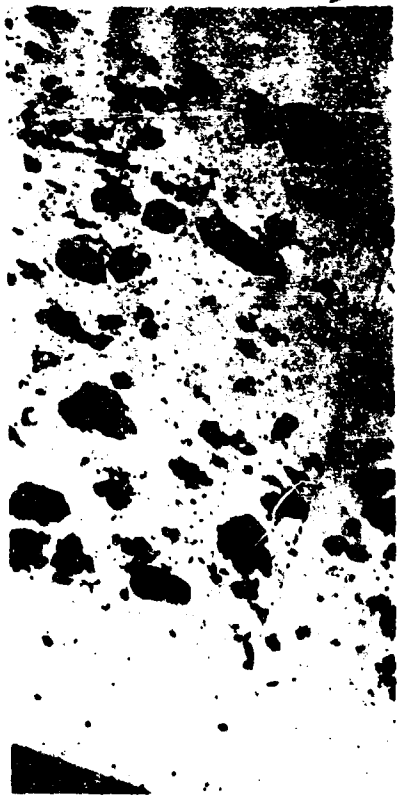
FIGURE 13. AS-FABRICATED PM-3A FUEL TUBE METALLOGRAPHY FUEL TUBE X3BK

metallography to detect variances in damage as a function of U-235 burnup. Six transverse and two longitudinal sections were cut from this fuel element. Two metallographic specimens were also cut from high performance fuel tube No. 12-90, one specimen from each of the high performance tubes C-1 and C-2, and one specimen from the average performance tube 12-102. Figures 14 through 23 show selected photomicrographs depicting eleven transverse and two longitudinal metallographical specimens cut from the fuel tubes.

Figure 14 shows results of clad and fuel matrix metallography, respectively, for fuel tube 12-46. The following comments can be made concerning the six metallographic specimens at the indicated positions for fuel tube 12-46.

1. Position B: No cracks were found in the clad at this position on fuel element 12-46. Figure 14B-1 shows a typical micrograph of the clad and clad-fuel matrix interface. No damage was noted to clad or clad-fuel interface. Depending on size and orientation of grains, between 3 to 6 grains spanned the cladding thickness. Figure 14B-2 shows a typical micrograph of a UO_2 particle. Some porosity was observed in the UO_2 particles at this location.

2. Positions D and E: Figures 14D-1 and 14E-1 show typical micrographs of the cladding and clad-meat interface at the D and E positions of fuel element 12-46. Discussions of D and E positions are combined because of similar results. The following comments apply to both positions on the fuel element:



100X As Polished HC18683



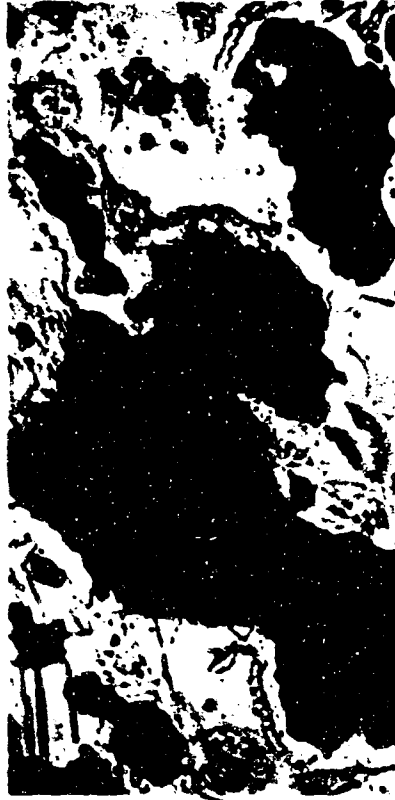
250X Etched HC19056



250X Etched HC19074



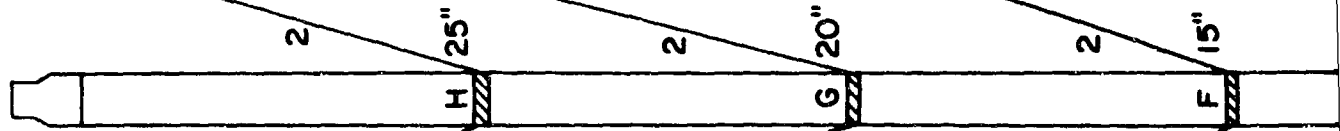
500X As Polished HC18682



500X Etched HC19063



500X Etched HC19081



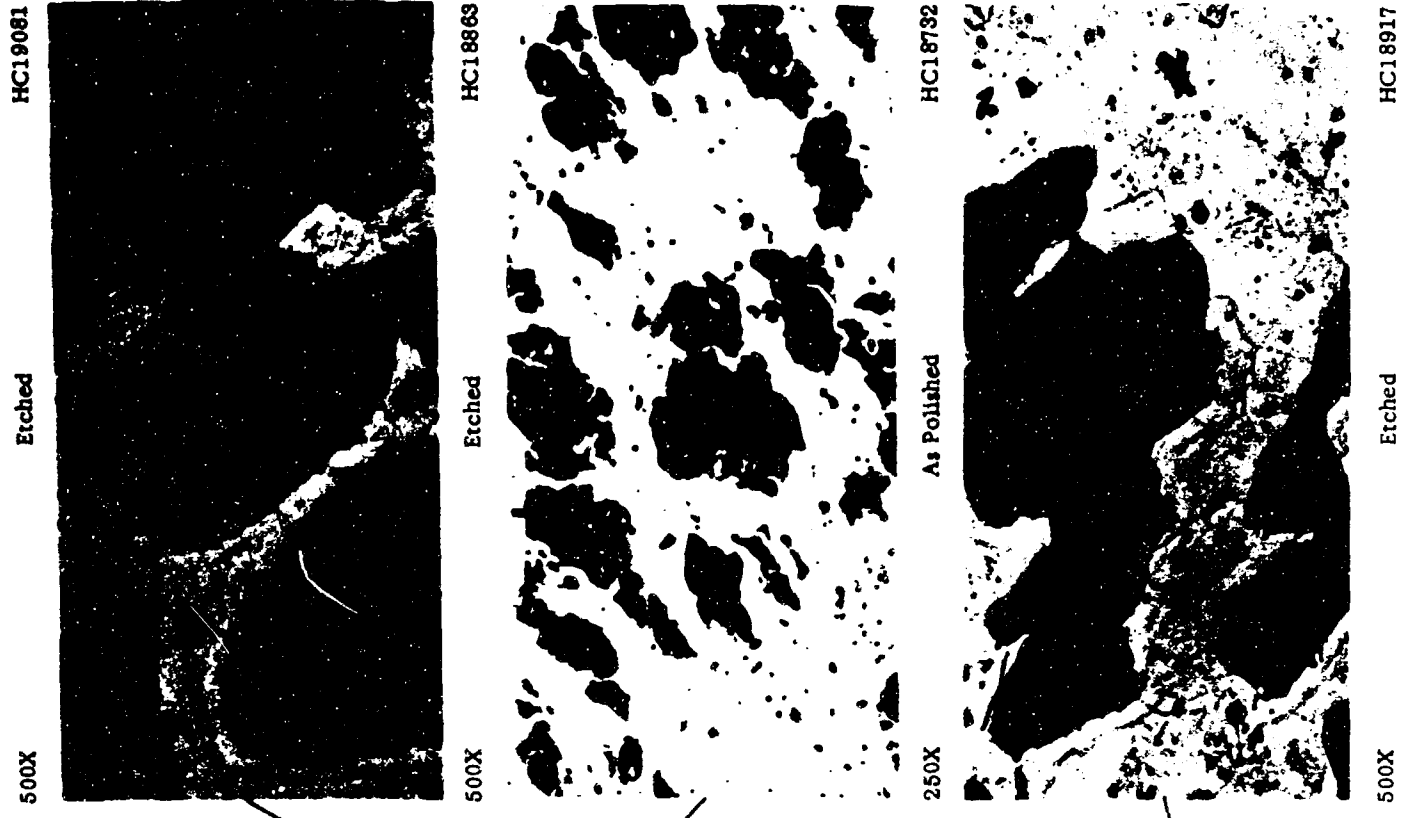
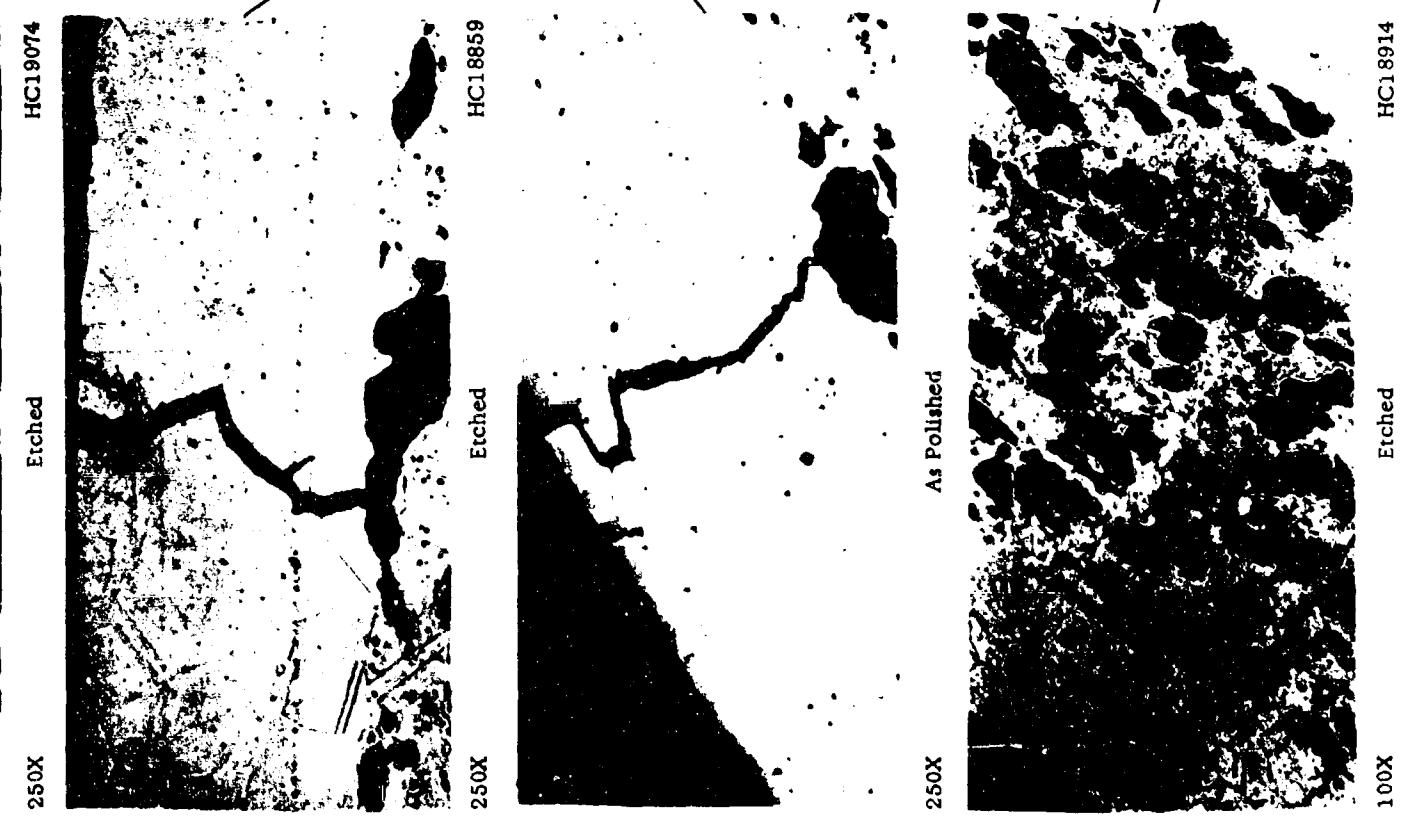


FIGURE 14. MICROSTRUCTURES OBSERVED AT SEVERAL POSITIONS IN FUEL TUBE 12-46

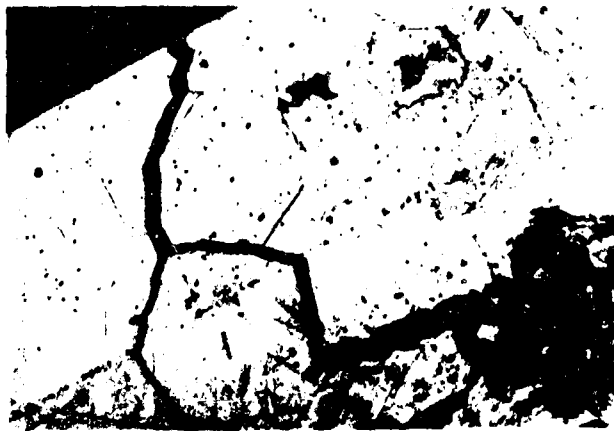
- a. About 30 cracks were detected around the periphery of the outer clad.
- b. Many cracks (about 1/3) were double at the outer edge and combined into a single crack at some point within the clad and continued as a single crack which terminated at a fuel particle.
- c. All cracks detected were intergranular.
- d. The cracks appeared to have been initiated at the outside edge of the outer clad since some smaller cracks were started at the outside edge of the clad but terminated before completely penetrating the clad.
- e. No cracks on the inner clad were observed.
- f. All cracks that penetrated the clad appeared to terminate at a UO_2 particle close to the clad-fuel interface.
- g. Grain boundaries appeared to be relatively free of precipitates, indicating that the stainless steel was not sensitized.
- h. In some cases, foreign material appeared in the cracks.
- i. Depending on the size of the grains and their orientation, the outer clad varied between 3 to 6 grains thick.
- j. The fuel dispersion appeared to be relatively undamaged.
- k. Clad and fuel matrix grain size appeared to be the same as observed in micrographs of unirradiated specimens.

Figures 14D-2 and 14E-2 show typical micrographs of the UO_2 fuel particles at the D and E positions, respectively. Note that the size of the porosity in the UO_2 particles has increased.

3. Position F: Figure 14F shows a typical micrograph of the clad and fuel matrix at the F position of fuel element 12-46. No crack in the cladding was found to penetrate completely through the clad at this position. The micrograph shown represents the worst clad condition found in this position.
4. Positions G and H: Figures 14G and 14H show typical micrographs of the cladding and fuel matrix at the G and H positions of fuel element 12-46. No cracks or other damage was noted to the cladding or clad-meat interface at this position. Note the absence of spherical porosity in the UO_2 particles.

Figure 15 is a selection of photomicrographs depicting various outer clad cracks found in the high performance fuel tube specimen 12-46-E. Morphology of the cracks in this specimen indicate that corrosive attack to the cladding may have played a role in inducing clad failure:

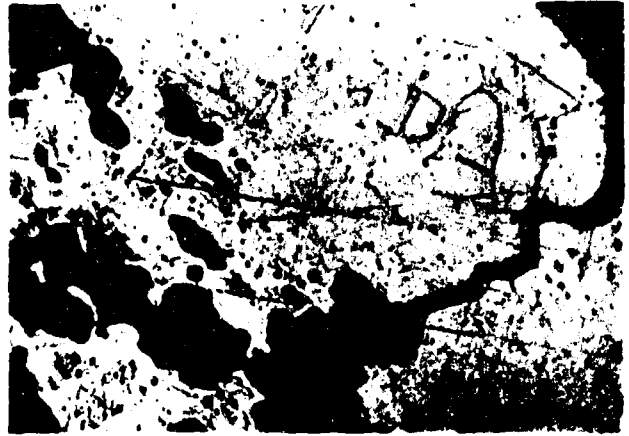
1. Branch-type cracking observed in the fuel tubes is indicative of stress-activated chemical attack, rather than purely mechanical cracking. One example of branch-type cracking is shown in Figure 15a.



250X

a. Etched

HC18857



250X

b. Etched

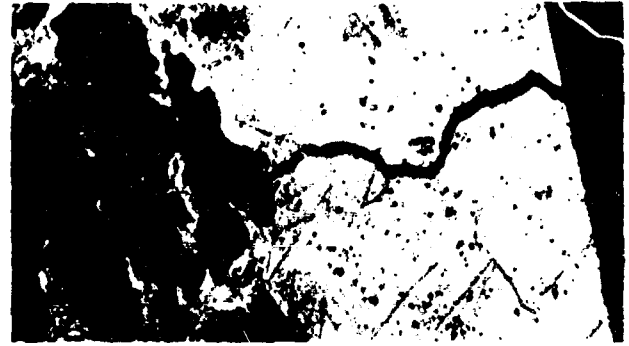
HC18858



250X

c. Etched

HC18861



250X

d. Etched

HC18863



250X

e. Etched

HC18864



100X

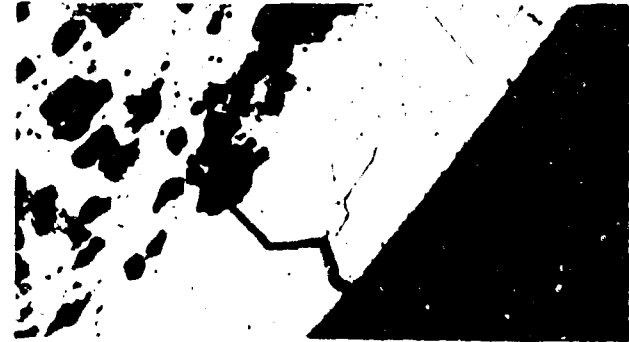
f. Etched

HC18871



100X

g. Etched



100X

h. Etched

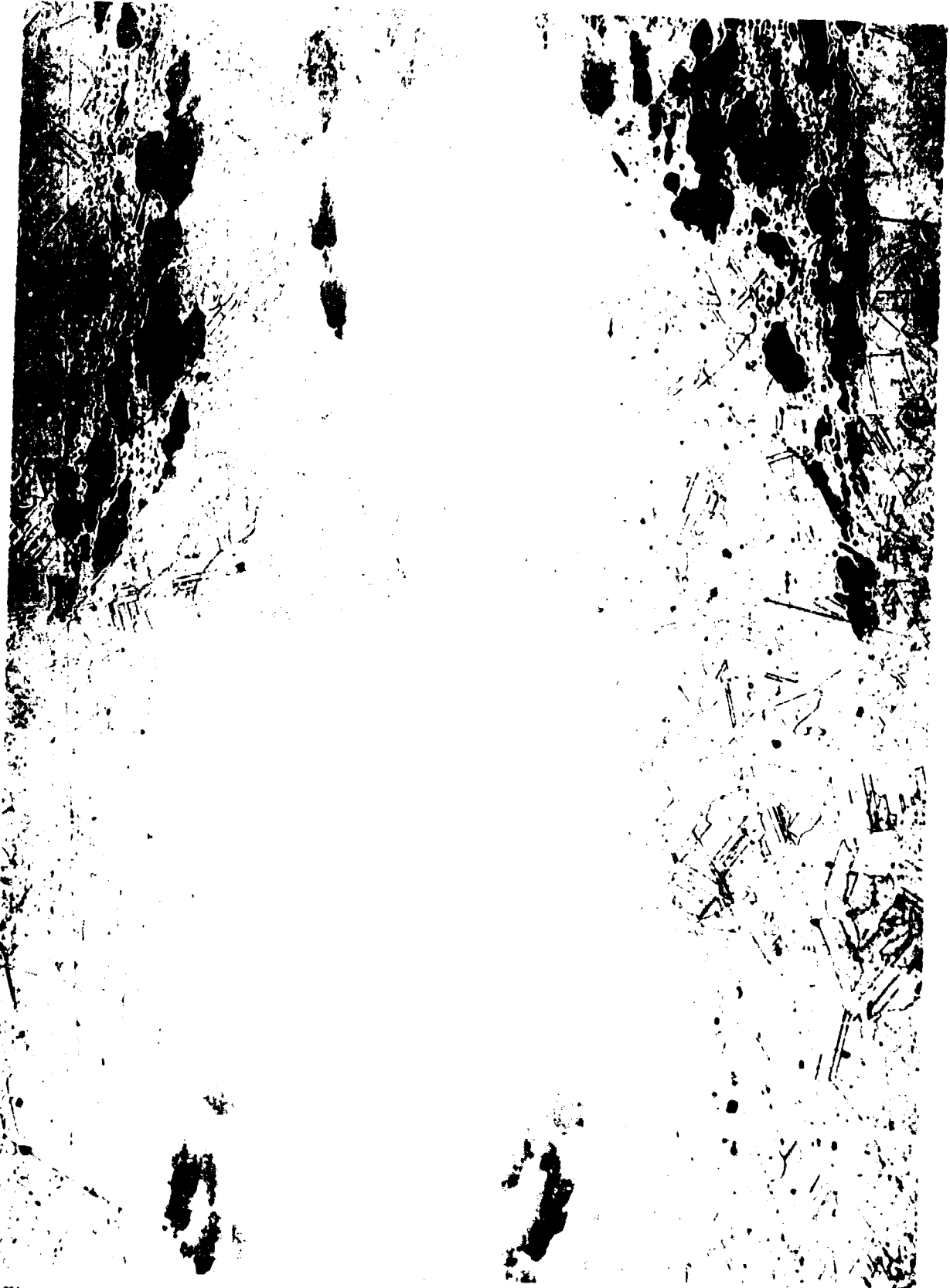
HC18872

FIGURE 15. SELECTED MICROGRAPHS DETECTING CLAD CRACKING IN SPECIMEN 12-46-E

2. One possible explanation to the loss of clad material in the clad crack as depicted in Figure 15c is grain annihilation by corrosive attack. Partial grain annihilation is exemplified by the small grain located adjacent to the cavity which is almost completely surrounded by intergranular attack. Also, the smaller crack that neighbors the major failure is further evidence that corrosive attack was occurring.

Figure 16 shows a photomicrograph composite of specimen 12-46-A, i.e., the longitudinal specimen cut from the lower fuel core-dead end interfaces of fuel tube 12-46. Microstructural examination of this region of a high-performance fuel tube was of importance because fuel bundle fabrication procedures might have produced non-bonded areas in this section. After inner and outer stainless steel-clad tubes were isostatically pressure-bonded to the sheathed UO_2 -stainless cermet tube, both ends of the composite tube were swaged to a smaller diameter. The lower tube end was then press-fitted into the fuel bundle lower grid, then roll expanded radially for a tight fit. It was felt that the extra deformation occurring in the lower end of each fuel tube could result in a loss of cermet-clad bond integrity, thus allowing an escape path for fission products.

No unbonded areas were found at or near this particular junction of cermet and end cladding. In fact, interdiffusion across the cermet cladding-end cladding interface was so complete that it was difficult to even detect



100x

Etched

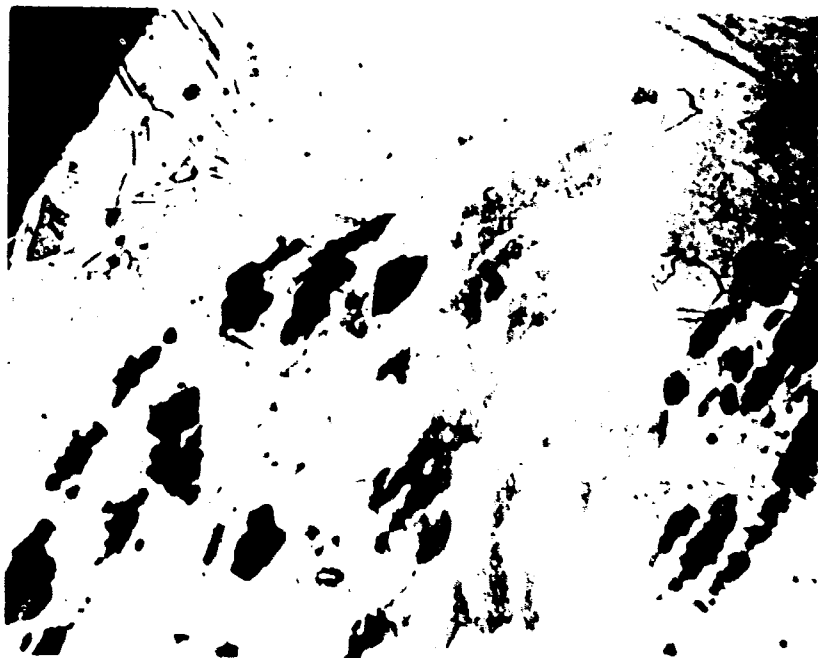
HC18646-HC18849

the interface. Several fuel particles were observed in the end clad region of the fuel tube. However, fuel particles were also found in this region in unirradiated PM fuel elements.⁽⁸⁾ Evidently, the transport of the UO_2 particles into the end clad region occurred during tube fabrication.

Figure 17 shows a representative photomicrograph of a section of the upper longitudinal specimen cut from the upper fuel core-dead end interface of fuel tube 12-46.

Figures 18a and 18b represent typical microstructures of fuel tube 12-90. Figure 18a shows a crack which extends into the outer clad approximately three mils. This was the only crack found on this specimen which was taken from the high performance region of fuel tube 12-90. Figure 18b shows the condition of the dispersion fuel in the vicinity of a UO_2 particle. An indication of second phase material was also observed in the UO_2 particle. Identification of the second phase was not attempted, since it seemed unlikely that the material contributed to clad failure. The 6-micron-thick band around the fuel particle probably reflects the fission product recoil range, rather than interaction between UO_2 and stainless steel.

Figures 19a and 19b show micrographs of a transverse specimen taken from a low performance region of fuel tube 12-90. No cracks or crack indications were found in the clad at this position on fuel tube 12-90. Also apparent is the lack of spherical porosity in the UO_2 . A recoil region was visible in the stainless steel matrix around the periphery of the UO_2 particles, Figure 19b.



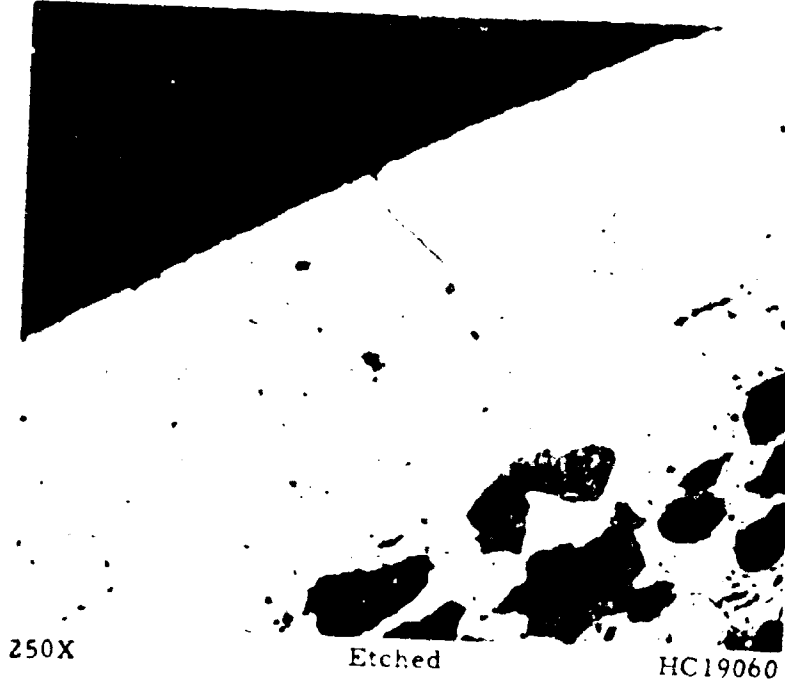
100X

HC18873

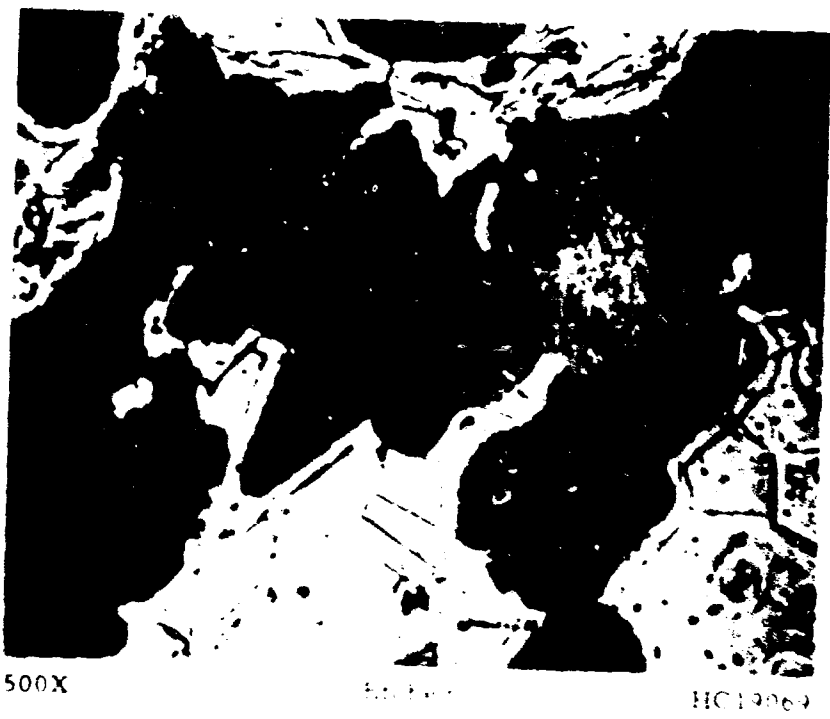
HC18873

FIGURE 17. TOP LEFT

12-46

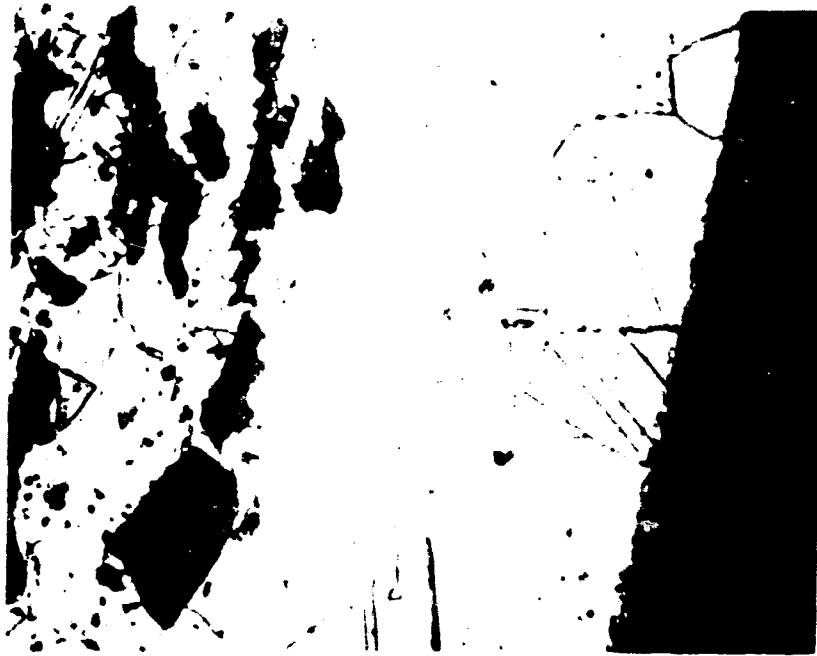


a. Clad, High-Performance Steel Specimen 12-90-E



b. Fine Detail of Clad, High-Performance Steel Specimen 12-90-E

FIGURE 1. CLAD, HIGH-PERFORMANCE STEEL SPECIMEN 12-90-E
 (a) 250X MAGNIFICATION (b) 500X MAGNIFICATION

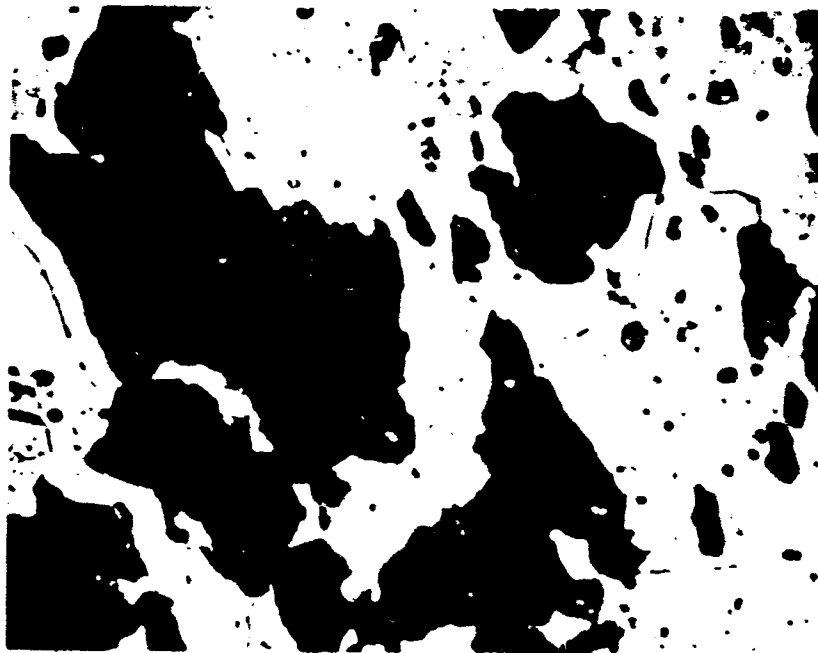


250X

Etched

HC19051

a. Typical Clad Microstructure - Low-Performance Region (Inner Part) - Tube 12-90



500X

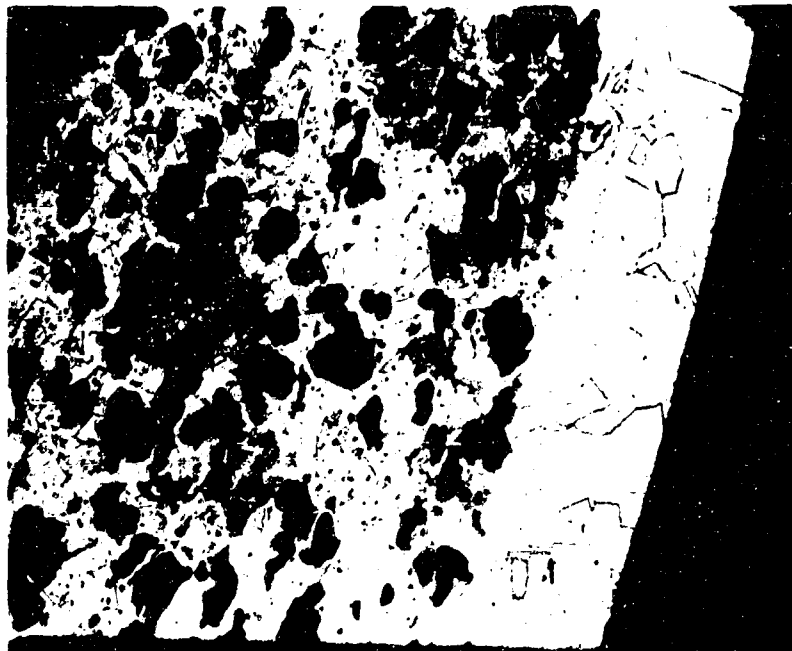
HC19052

b. Typical Fine Microstructure - Low-Performance Region (Inner Part) - Tube 12-90

FIGURE 10. METALLOGRAPHIC MICROSTRUCTURES OF THE LOW-PERFORMANCE REGION OF TUBE 12-90

Figures 20a and 20b are micrographs of a transverse specimen taken from fuel tube 12-102 at the E position. Figure 20a shows the clad condition at this position. No cracks or crack indications were found in the clad at this average performance position on fuel tube 12-102. Relatively large quantities of fission gas bubbles were present in the UO_2 particles in this region, Figure 20b.

Figures 21 and 22 show results of metallography on two fuel tubes taken from the center bundle. These fuel tubes were located in positions of equal symmetry within the center bundle. Both transverse specimens were cut from the high performance region of both fuel tubes. Figure 21 is composed of a photomicrograph composite of specimen C-1-E with higher magnification micrograph inserts depicting selected clad cracks. Note that there appears to be no preferred pattern as formed by the clad crack positions located within the outer clad. Again, cracks were intergranular in nature, and limited to the outer clad tube. Figure 22 shows selected micrographs depicting microstructure of the specimen taken from the high performance domain of fuel tube C-2, i.e., specimen C-2-E. Figure 22a, and -b are micrographs of the same clad crack. Note that the crack is intergranular and terminates at the surface of a UO_2 particle resulting in an open path between cooling water and fission products. Figure 22c and -d illustrate two more examples of intergranular cracking terminating on the surface of a UO_2 particle. Apparently the void in the stainless steel matrix caused

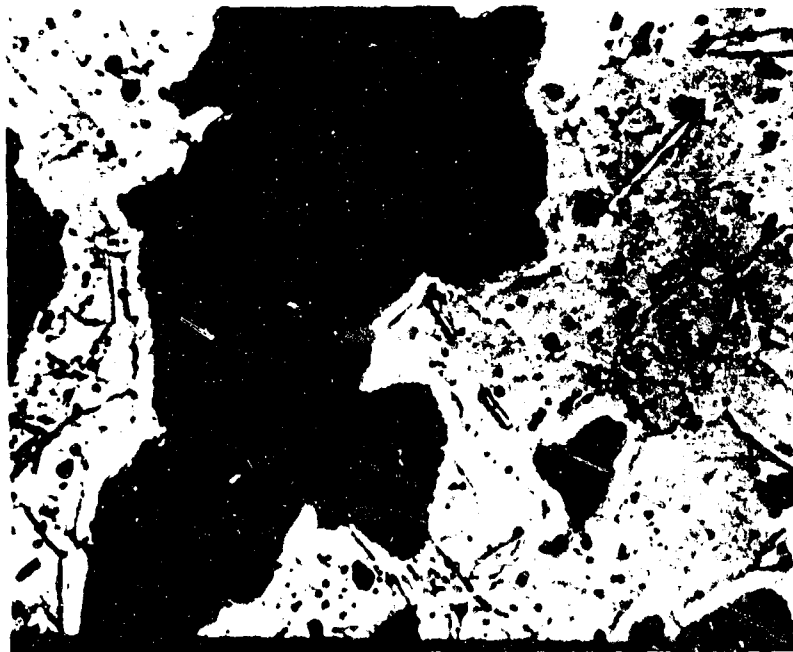


100X

Etched

HC18918

a. Dispersion Clad



500X

Etched

HC18922

b. UO₂ Particle and Stainless Steel Matrix

FIGURE 20. TYPICAL MICROGRAPHS FOR SPECIMEN 12-102-E

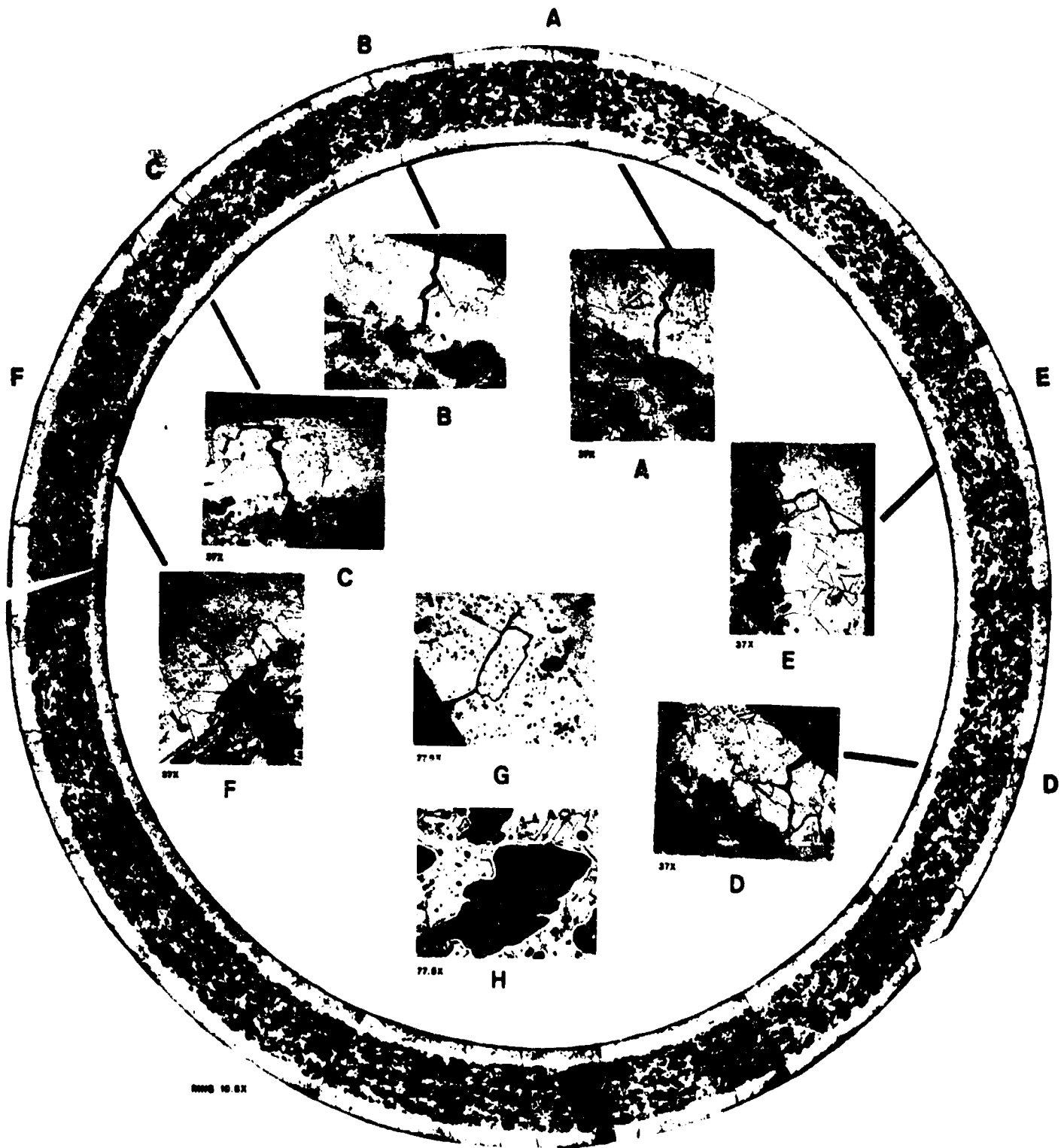
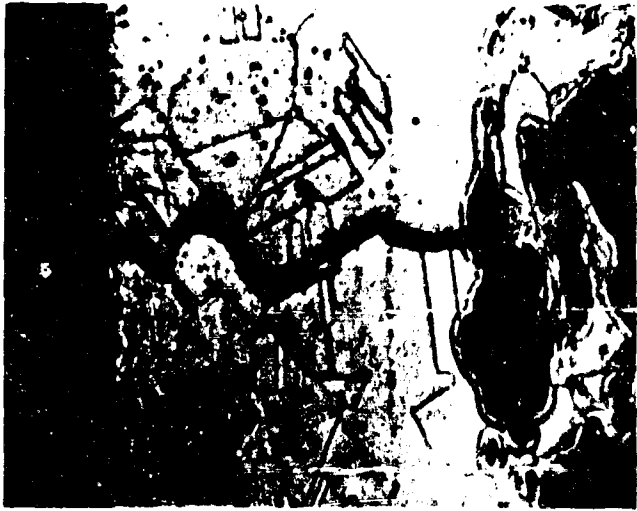


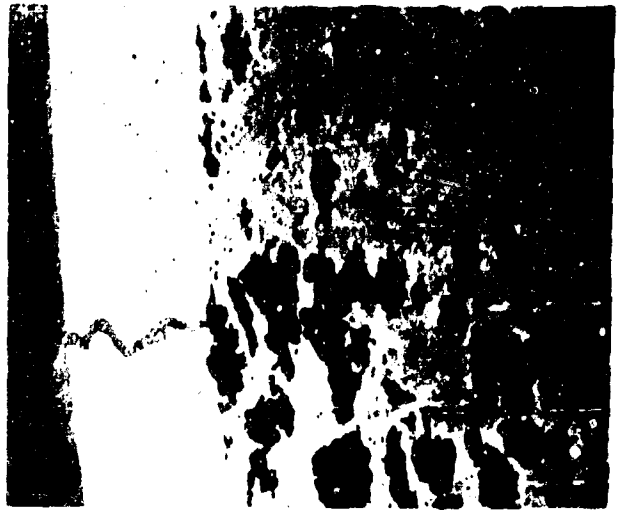
FIGURE 21. MICROGRAPH COMPOSITE OF FUEL-TUBE SPECIMEN C-1-E WITH HIGHER MAGNIFICATION INSERTS



250X

a. Etched

HC19191



100X

b. As Polished

HC19099



250X

c. Etched

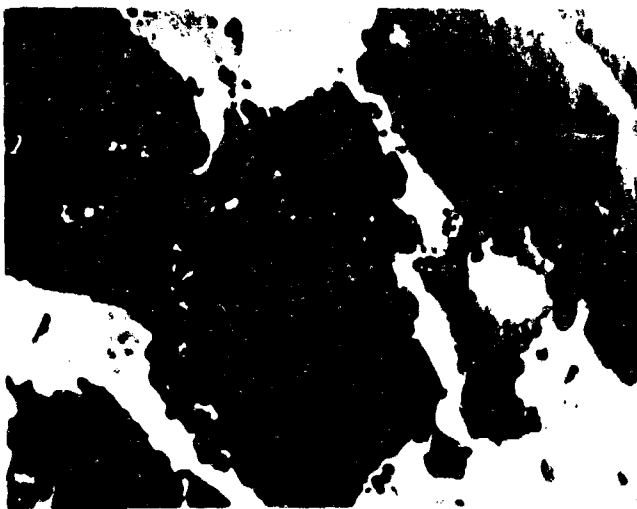
HC19190



250X

d. Etched

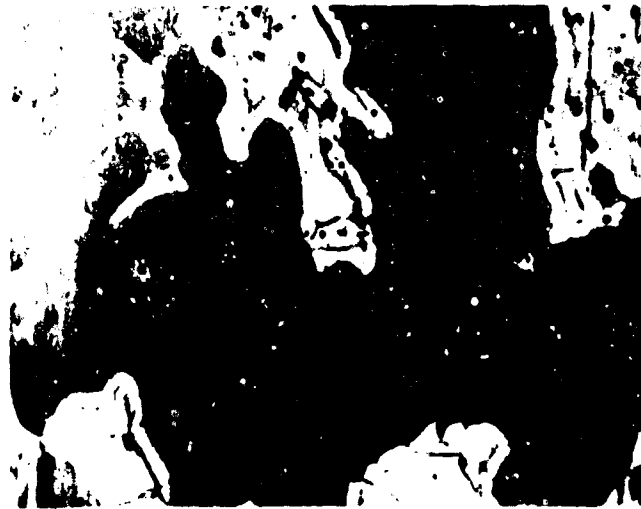
HC19162



500X

e. As polished

HC19190



500X

f. Etched

HC19146

FIGURE 22. SELECTED MICROGRAPHS OF THE MICROSTRUCTURE OF SPECIMEN C-2-E

by the presence of a UO_2 particle acts as a crack arrester. The stress concentration at the crack notch is reduced significantly when the crack notch reaches the surface of a UO_2 particle.

Figure 23 shows two photomicrograph composites depicting two of the many outer clad tube cracks detected in specimen C-2-E. Of special interest here is the fact that some unidentified material appeared to be lodged within the clad cracks, Figure 23a and -b. It appears that the foreign material lodged within the crack was one or both of the following:

1. UO_2 that had extruded, or in some other manner been transported, into the crack, or
2. Products of stainless steel corrosion.

In an attempt to identify the material present in the clad cracks, autoradiographs were taken of metallographic specimen C-2-E to detect the presence of uranium alpha activity in the crack. No evidence of uranium alpha activity in the cracks was detected. The results suggest that the material was not alpha active and hence, is probably a stainless steel corrosion product that formed when the crack surface was exposed to reactor coolant. Furthermore, Figure 23b shows that the foreign material was lodged within a smaller branch crack, the direction of which probably was not susceptible to an influx of material moving out through the trunk crack.



500X

HC19147-HC19149

a. Etched



500X

HC19150-HC19151

b. Etched

FIGURE 23. PHOTOMICROGRAPH COMPOSITE SHOWING TWO OF THE CLAD-TUBE CRACKS IN SPECIMEN C-2-E

Void Fraction in UO₂ Particles. The void fraction in selected UO₂ particles contained in eight metallographic specimens was measured after irradiation by point counting techniques.⁽⁹⁾ In this technique, a systematic array of points, formed by the corners of a two-dimensional lattice, was placed over the photomicrograph of a given UO₂ particle. The number of points falling over a void were then counted. The void volume fraction present in the UO₂ particle was calculated by dividing the number of counted points located over voids by the total number of points in the given area. Table 4 gives the results generated by the above procedure.

TABLE 4. VOID FRACTION IN UO₂ FUEL PARTICLES

Metallographic Specimen No.	Estimated Burnup Fissions/cm ³ x 10 ²⁰	UO ₂ Particle Void Fraction, percent
12-46-B	6.5	16
12-46-D	14.6	24
12-46-E	14.8	26
12-46-F	7.6	18
12-90-E	14.0	28
12-102-E	10.0	20
C-1-E	15.1	35
C-2-E	15.1	38

The fraction of porosity in the UO_2 particle as a result of irradiation was highest in high performance regions of the fuel tubes, indicating that the fuel volume increase was greatest in these regions. It was in these regions that the clad exhibited the greatest population of cracks, indicating that stress induced in the cladding as a result of fuel swelling was a factor in producing the cracks.

Because of the possibility that scale buildup may have affected the micrometer measurements of the tube diameters, the increase in diameter of fuel tube 12-46 in the maximum burnup region was estimated from the measured increase in void volume in the UO_2 particles. Assuming isotopic swelling of the fuel and an initial UO_2 fuel particle density of only 90 percent of theoretical, these estimates indicate that the fuel tube diameter increased about one percent. This estimated increase is larger than the increase of about 0.6 percent calculated from the diameter measurements.

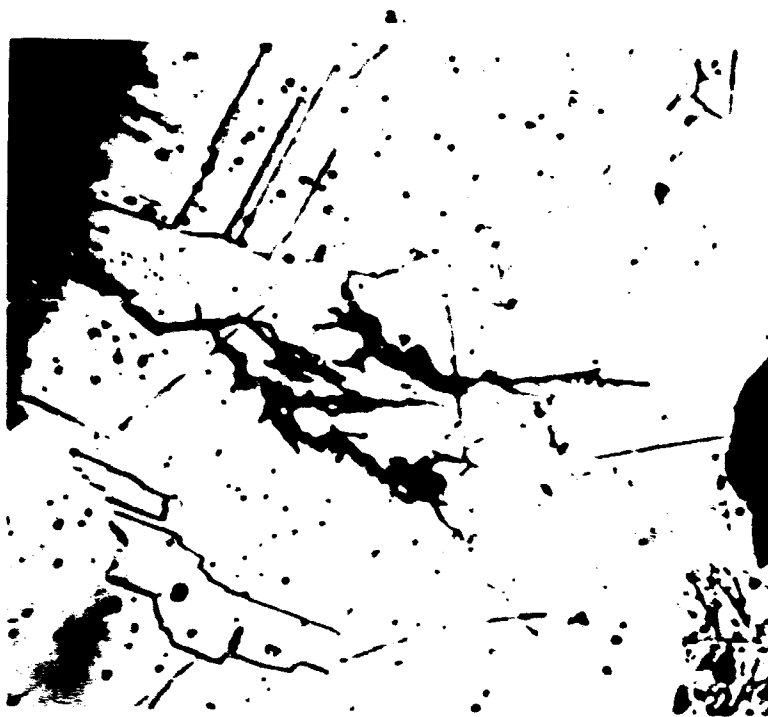
Chloride-Treated Fuel Tube. The cladding of chloride-treated fuel tube 12-139 which was removed from a low-performance region of the core was metallographically examined for cracks. No visual evidence of cracking was observed on fuel tube 12-139 prior to treatment. As shown in Figure 24, transgranular cracks typical of chloride-induced stress-corrosion cracking⁽¹⁰⁾ were found only in the outer cladding. The



500X

Etched

HC19016



500X

Etched

HC19024

b.

FIGURE 24. PHOTOMICROGRAPHS OF FUEL TUBE 12-139 AT STRESS ACTIVATED-CHLORIDE CORROSIVE ATTACK TO GLAD ON FUEL TUBE 12-139

difference in crack morphology gives some indication that the intergranular attack detected in the as-irradiated PM-3A fuel tubes was not primarily activated by chloride.

Scale Analysis

Exposure of Type 347 stainless steel to high temperature and reactor grade water resulted in the formation of a dark oxide surface film. Breden⁽¹¹⁾ points out that autoclave and loop corrosion tests gave evidence that 18% Cr and 8% Ni stainless steels contributed a considerable amount of corrosion products to the water.

Physical Characteristics of Suspended Scale. The black crud burst experienced in the storage pool upon opening of the shipping cask is considered typical of the behavior observed with pressurized water reactors and a Battelle-Columbus water loop. Experience at Battelle⁽¹²⁾ has shown that a newly-opened post-operated loop will discharge a finely divided black product which was determined by analysis to be a Fe_3O_4 -type oxide.

Adherent-Scale, X-Ray Diffraction Analysis. X-ray diffraction traces of scale samples showed lines appearing at two-theta values of 35.4° and 43° two theta corresponding to interplanar spacings of 2.53\AA and 2.1\AA . These interplanar spacings correspond to two of the interplanar spacings of magnetite, Fe_3O_4 .⁽¹³⁾

Suspended Scale, X-Ray Spectrographic Analysis. Qualitative X-ray spectrographic analysis of a sample of the black scale taken from the as-received PM-3A shipping cask showed the presence of Fe, Cr, Ni, and small amounts of Cu, Zn, and Pb. No europium was found. The trace amounts of copper, zinc and lead may have been introduced into the system as a result of corrosion of the brass hardware that is part of the pressure relief device attached to the upper cask plumbing.

Nuclide Composition of Scale. Gamma ray spectrometer analysis of the black scale taken from a shipping cask water sample showed the nuclides to be Fe^{59} , Co^{58} , Mn^{54} , Co^{60} , and Y^{91} . All of these nuclides are a result of neutron activation of stainless steel with the exception of Y^{91} , which is a fission product. Cobalt-58 is created by the (n,p) reaction with the target nuclide Ni^{58} ; Cobalt-60 is created by the (n, γ) and (n,p)

reactions with the target nuclides Co^{59} and Ni^{60} , respectively; iron-59 is created by the (n,γ) reaction with target nuclide Fe^{58} ; and manganese-54 is created by the (n,p) reaction with the target nuclide Fe^{54} . All target nuclides mentioned above are, of course, constituent elements in the core material stainless steel. Other radioactive nuclides are formed during the neutron irradiation of stainless steel, but the four above nuclides are the most plentiful, long-lived radioactive nuclides.

Scale Color and Adherent Physical Characteristics. All visible scale associated with the PM-3A core (suspended in the shipping cask water and adhered to the core surfaces) was black in color. Depending on the amounts of oxygen dissolved in the water, aqueous stainless steel corrosion products may take on several colors. Stainless steel 18% Cr - 8% Ni systems in 400 F to 600 F water with low dissolved oxygen content produce largely black crystalline magnetite (Fe_3O_4).⁽¹¹⁾ With higher oxygen concentrations, $\alpha\text{Fe}_2\text{O}_3$ is formed and the oxide appears reddish brown in color and is less adherent.

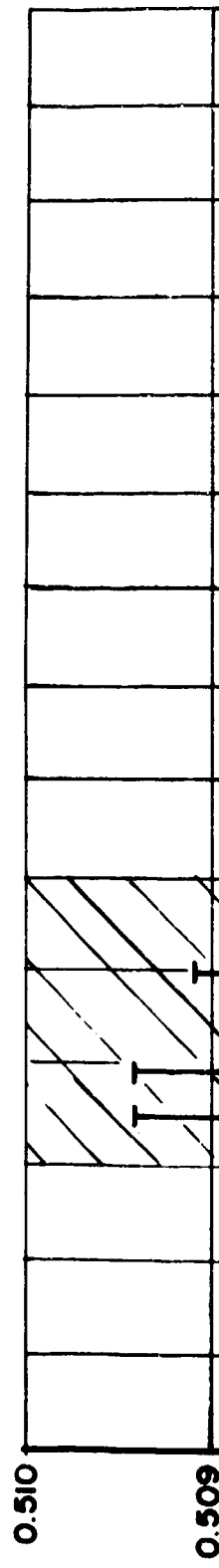
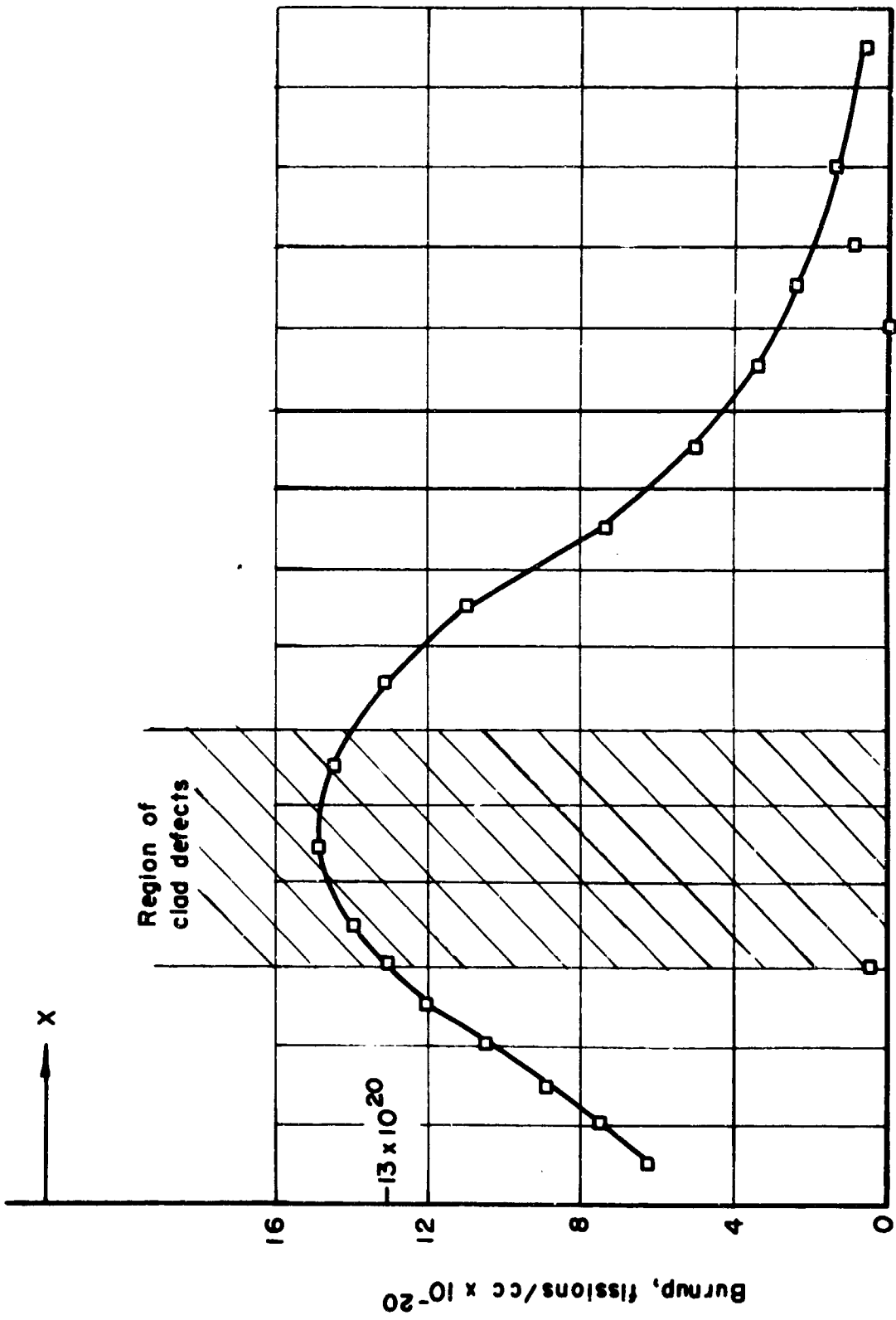
The scale found on the PM-3A fuel tubes was probably corrosion product deposition under radiation, which is typical in pressurized water reactors.

DISCUSSION

The major objectives of this program were to find the leaking fuel tubes and to determine the cause(s) of the leaks.

The results of the examination indicated that the fission products leaked through numerous intergranular cracks in the outer clads of fuel tubes from the high-performance region of the core (toward the core center). These cracks started on the outer surface of the clad and generally terminated at UO_2 particles near the fuel dispersion-clad interface. All the cracks were longitudinal, suggesting their association with hoop stresses. As shown in Figure 25, the cracks occurred only in high-performance regions of the fuel tubes where burnups exceeded about 13×10^{20} fissions/cm³ and where fuel swelling produced strains of about one percent in the clad.

The cause of the failure is not clear. Based on the results of irradiation tests of plate specimens, other investigators⁽¹⁴⁾ have predicted failure of UO_2 -stainless steel dispersions as a function of burnup and temperature as shown in Figure 26. Based on the data shown in Figure 26, and a burnup of 13×10^{20} fissions/cm³ and a surface temperature of 620 F, the PM-3A, Type 1 Serial 2 Core clearly operated in the probably-stable-region of the plot for this type of fuel. Perturbations to heat flow introduced by the oxide scale on the PM-3A fuel tube surfaces may have raised fuel operating temperature slightly and shifted the operating point toward the stable-unstable boundary. However, it seems unlikely that the presence of the scale could



A

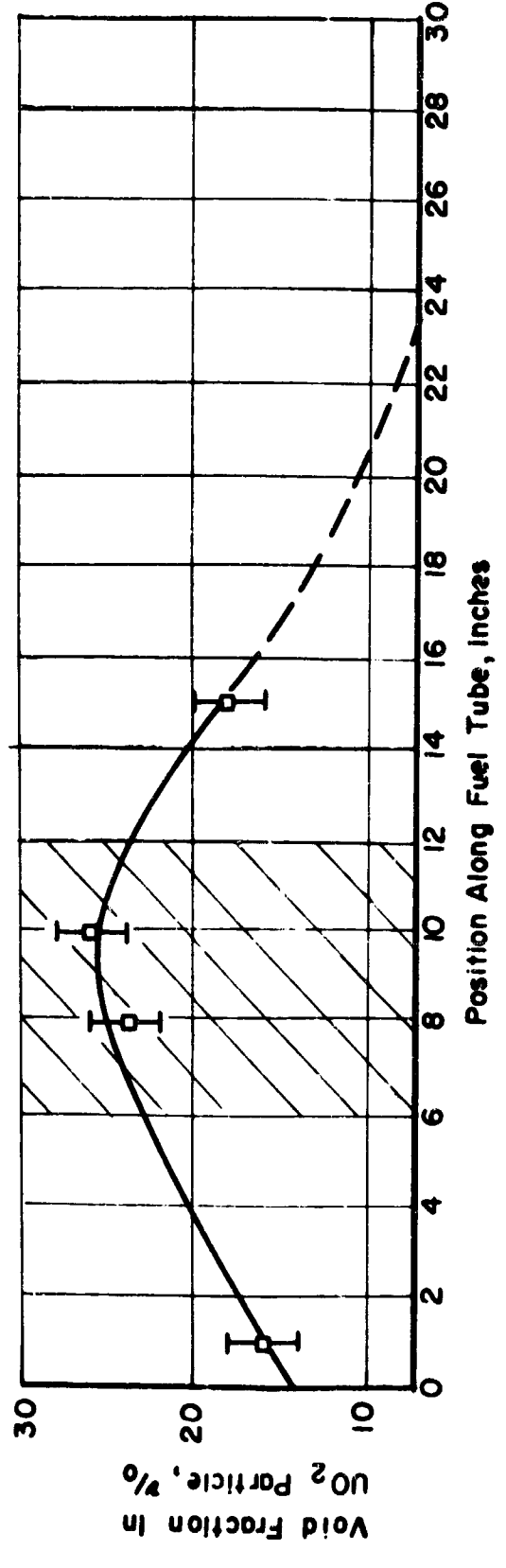
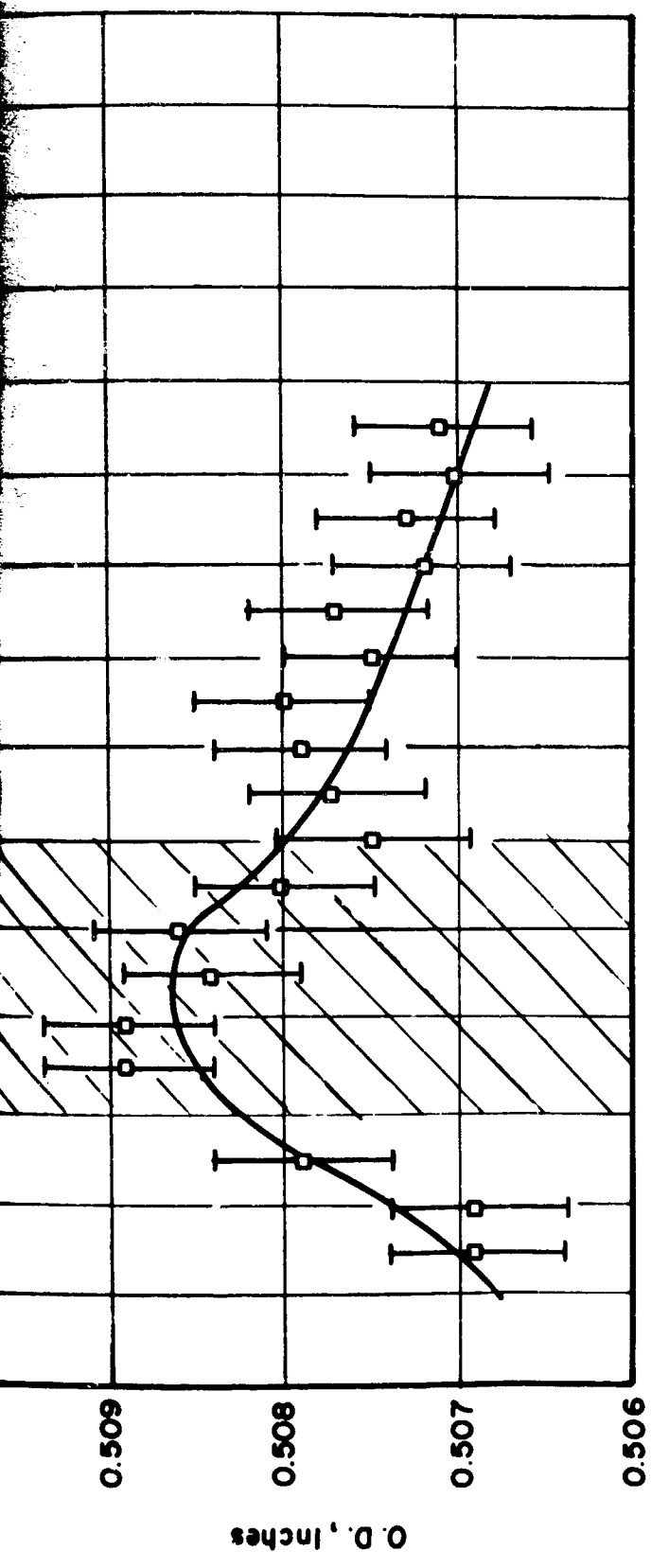


FIGURE 25 RELATIONSHIP OF FUEL BURNUP, FUEL PIN SWELLING AND VOID FRACTION IN UO_2 PARTICLES TO FORMATION OF CLAD DEFECTS IN FUEL TUBE 12-46

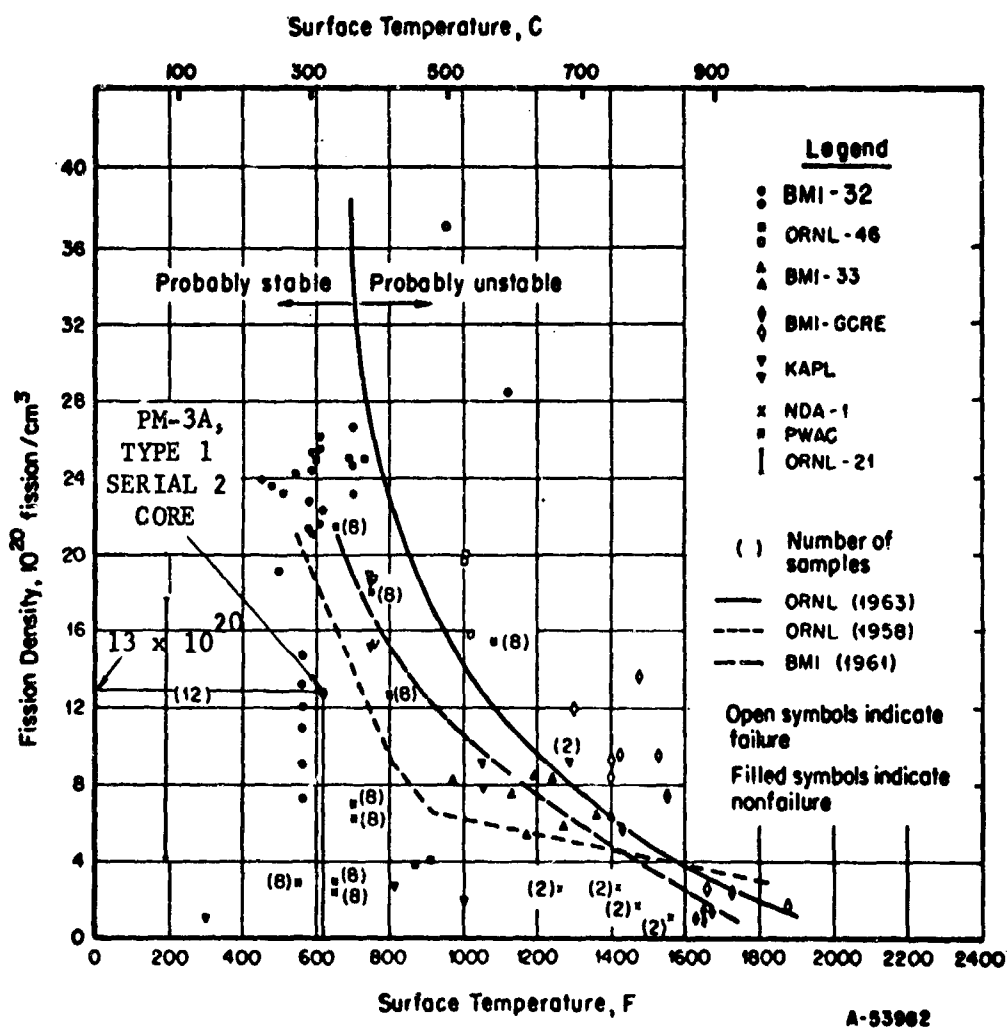


FIGURE 26. IRRADIATION PERFORMANCE OF STAINLESS STEEL-UO₂ DISPERSIONS⁽¹⁴⁾

have raised temperature sufficiently to bring the operating conditions into the non-stable region of the data shown in Figure 26.

Neutron irradiation is, of course, known to significantly reduce the ductility of stainless steels. Based on high-strain rate data, it is difficult to reconcile the observed cracks in the PM-3A fuel tubes with neutron embrittlement. At most, the PM-3A clad received a total neutron dose of 10^{21} nvt. In short-time, high-strain rate tensile tests at 600 F, Type 347 stainless steel specimens irradiated to neutron exposures greater than 10^{21} nvt, elongated 10 to 15 percent before rupturing.⁽¹⁵⁾ This elongation to cause rupture is at least an order of magnitude higher than the calculated one percent deformation in the defected region of the outer clad on the PM-3A fuel tubes. However, it is possible that the cladding ductility may have been adversely affected by the very low strain rate (10^{-8} in./in./min.) experienced by the PM-3A outer clad, as compared to the high strain rates used to generate the quoted data on irradiated Type 347 stainless steel. Ductility of materials in creep is generally lower than that observed in short-time tension tests.

Careful examination of crack morphology indicated that chemical attack may have played a role in crack propagation. Coupling these observations with the previously mentioned strain dependence of failure suggests that clad failure may have been induced by some stress-accelerated chemical attack. Such attack could not be attributed to sensitization, since there

was no evidence of grain boundary precipitation in the clad. The two common environmental causes of stress corrosion in stainless steel are chlorides and caustic. Chloride stress-corrosion cracking of austenitic stainless steels is generally associated with localized concentrations of chloride in the environment. In this case, a purely chloride attack can be discounted for two reasons: (1) chloride content of the water was low, and there was no obvious means whereby the chloride could become concentrated (such as localized boiling) and (2) all cracks observed were intergranular, whereas chloride-induced stress-corrosion cracks in non-sensitized austenitic stainless steel are normally transgranular.

Caustic stress corrosion cracking occurs in strong bases such as NaOH, KOH, and LiOH. The only known source of hydroxyl ions in the PM-3A reactor coolant was the NH_3 used for pH control. Based on present knowledge, ammonia does not cause stress corrosion cracking of stainless steels and thus would not be considered a factor in the cracking failures observed.

At least two other investigators, Lees⁽¹⁶⁾ and Staehle,⁽¹⁷⁾ have reported failures by intergranular cracking of stainless steel under environmental conditions existing in boiling-water reactors. Both investigators proposed a chemical-mechanical mechanism of failure but neither investigator could identify the chemical factor. On the other hand, there has been considerable trouble-free operating experience with stainless-steel-clad fuels in pressurized-water reactors.

CONCLUSIONS

Conclusions reached as a result of the examination of the Type 1 Serial 2 PM-3A core are as follows.

Fission product buildup in the primary reactor coolant resulted from leakage through intergranular cracks in the outer clad. The cracks started at the outer clad surface and terminated at UO_2 particles in the UO_2 -stainless steel dispersion fuel. All observed cracks were longitudinal in direction and were located in the high-performance regions of fuel tubes located toward the core center where fuel burnup exceeded about 13×10^{20} fissions/cm³ and clad stress was greatest. It was not possible to positively identify the cause of cracking because of the complex environmental factors. Neutron embrittlement of the clad was undoubtedly a factor, but the amount of strain associated with the failure was much lower than that expected to cause failure based on data available from stainless steel irradiations. The additional decrease in ductility may have been due to the very low strain rates (10^{-8} in./in./min.) and to the biaxial stresses to which the clad was subjected.

However, all factors considered in this limited investigation suggest the most probable cause of clad cracking was a stress-accelerated chemical attack of unknown origin.

FUTURE WORK

The results of this study, and the fact that the PM-1 and PM-3A Serial 1 Type 1 cores are also leaking fission products, indicate that some factor inherent in the PM-type reactor design or operation may be causing the fuel tube cladding to crack prematurely. This type of cracking of the clad has not been observed in other pressurised water reactors, although it has occurred in boiling-water reactors. It is recommended that an experimental program be initiated to establish whether the cracks are caused by an operational factor. If an operational factor is involved, the new core design just completed for FEC may not eliminate the problem.

It is suggested that at least one fuel bundle from PM-1 be examined to determine if the fission product release from this core is also the result of intergranular clad cracking. Since this core operated for about 15,000 hrs, with a correspondingly higher burnup than the PM-3A Type 1 Serial 2 core, it will be possible to further assess the extent of fuel swelling and associated clad strain required to produce cracks in the clad. If a stress-accelerated chemical process is involved, the longer operational time on the PM-1 core may produce more tangible evidence of the chemical factors which are involved.

REFERENCES

1. Monthly Operating Report for PM-3A Nuclear Power Plant McMurdo Station, Antarctica, Prepared by U. S. Naval Nuclear Power Unit, P. O. Box 96, Fort Belvoir, Virginia, Report No. 6, November 1-28, 1964.
2. Monthly Operating Report for PM-3A Nuclear Power Plant McMurdo Station, Antarctica, Prepared by U. S. Naval Nuclear Power Unit, P. O. Box 96, Fort Belvoir, Virginia, Report No. 3, August 2 to 29, 1964.
3. Description of PM-1 (Sundance), Reactor File No. 12, "PM-1 on the Line", Nucleonics, Vol 20, No. 9, p 37-42, September 1962.
4. Goslee, D. E., "Improving Performance of Stainless-Steel-UO₂ Cermet Fuels", Nucleonics, Vol 21, No. 7, p 48-52, July 1963.
5. O'Brien, J. F. (Project Engineer), "PM-1 Critical Experiments and Zero Power Testing", MND-M1858, Nuclear Division, Martin Company, Baltimore, Maryland, September 1961.
6. PM-3A Water Chemistry and Radiochemistry Support Team Report for Nuclear Power Field Office U. S. Army Engineer Reactors Group, Fort Belvoir, Virginia, NUS-228, Nuclear Utility Services, Inc., Washington, D. C., April 1, 1965.
7. Monthly Operating Report for PM-3A Nuclear Power Plant McMurdo Station, Antarctica, Prepared by U. S. Naval Nuclear Power Unit, P. O. Box 96, Fort Belvoir, Virginia, Report No. 7, November 29, 1964, to January 2, 1965.
8. Hobson, D. O., et al, "Characterization of Army PM-1 Type Reactor Fuel Elements", ORNL-TM-1676, Oak Ridge National Laboratory, December 1966.
9. Hilliard, J. E., and Cahn, J. W. "An Evaluation of Procedures in Quantitative Metallography for Volume-Fraction Analysis", Transactions of the Metallurgical Society of AIME, Vol 221, p 344-352, April 1961.
10. Berry, W. E., "Some Facts About Stress Corrosion of Austenitic Stainless Steels in Reactor Systems", Reactor Materials, Vol 7, No. 1, Spring 1964.

11. Breden, C. R., "Behavior of Reactor Structural Materials From the Standpoint of Corrosion and Crud Formation", TID-7587, AEC-Euratom Conference on Aqueous Corrosion of Reactor Materials, Brussels, Belgium, October 14-17, p 48, 1959.
12. Private Communication with Battelle-Columbus Staff Member, Warren E. Berry, May 17, 1966.
13. ASTM Diffraction Data Card Number 11-614.
14. Thurber, W. C., et al, "Irradiation Testing of Fuel for Core B of the Enrico Fermi Fast Breeder Reactor", ORNL-3709, November 1964.
15. Private Communication with Battelle-Columbus Staff Members F. R. Shober and M. Kangilaski.
16. Lees, E. A., "Analysis of Failure of Type 304 Stainless Steel Clad Swaged Powder Fuel Assembly, GEAP-4400, Vallecitos Atomic Laboratory, General Electric Company, San Jose, California, October 3, 1963.
17. Staehle, R. W., "Investigation of Cracking in Stainless Steel Fuel Elements", Report No. COO-1319-30, Topical Report by The Ohio State University Research Foundation to the U. S. AEC, Chicago Operations Office, Argonne, Illinois, October 25, 1965.

ACKNOWLEDGMENTS

This work was conducted under contract NBy-63910 for the Department of the Navy, Facilities Engineering Command. Liaison was maintained with Mr. James E. Bocock, of FEC, whose assistance was greatly appreciated. Core operating data obtained from the U. S. Naval Nuclear Power Unit was also greatly appreciated. The authors wish to express their appreciation to Professor Roger W. Staehle, Department of Metallurgical Engineering, The Ohio State University, Columbus, Ohio, and Mr. Warren E. Berry of the Battelle-Columbus Corrosion Research Division, and Mr. Fred R. Shober of the Battelle-Columbus Environmental Engineering Division for their helpful suggestions in the interpretation of the results obtained in this work. Many thanks are also extended to the Battelle Hot Cell Staff, whose dedicated efforts made the remote examination of the PM-3A core possible.

APPENDIX A

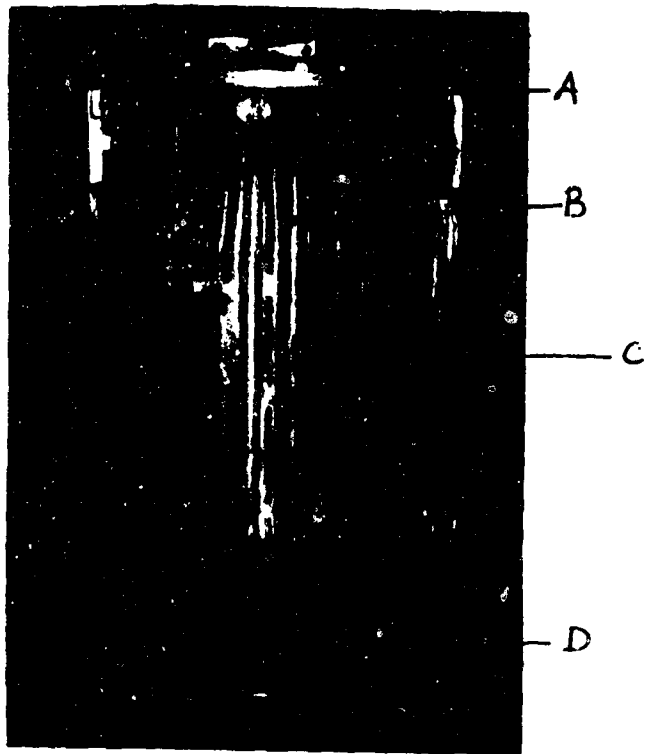
SHIPPING PACKAGE EXAMINATION AT BATTELLE-COLUMBUS

The following tasks were performed by Battelle in regard to the PM-3A shipping package:

- (1) Determine cask body temperature
- (2) Determine cask fin temperature
- (3) Determine cask water temperature
- (4) Determine cask pressure
- (5) Determine gamma energy spectrum of decaying fission and corrosion products present in the cask water
- (6) Take appropriate photographs of the shipping cask and associated hardware to show any damage or indicate areas needing repair.

Figure A-1 shows the spent fuel shipping cask with notation of areas of temperature measurement. Measured cask body and fin temperatures at several locations on the cask surface are shown in Table A-1. Measurements were performed with and without crash frame and shroud plate in place. All measured temperatures were less than 10°F above ambient temperature (71°F).

Locked compartments (two) located on the upper and lower side of the cask were opened to permit access to the gas release valve and water



TE00371

FIGURE A-1. PM-3A SHIPPING-CASK TEMPERATURE-MEASUREMENT POSITIONS

TABLE A-1. FM-3A SHIPPING CASK FIN AND BODY TEMPERATURES

Location on Cask (See Figure A-1)	Temperature* , Crash Frame and Shroud Plate in Place (F)	Temperature** , Crash Frame and Shroud Plate Removed (F)
Top at Body Position A	81	81
10 inches down from Flange, Position B		
Body	77	80
Fin-middle	77	78
Fin-edge	77	77
Middle of Cask, Position C		
Body	82	81
Fin-middle	82	79
Fin-edge	82	79
Bottom of Cask, Position D		
Body	78	78
Fin-middle	78	78
Fin-edge	78	78

* Ambient temperature - 70 F

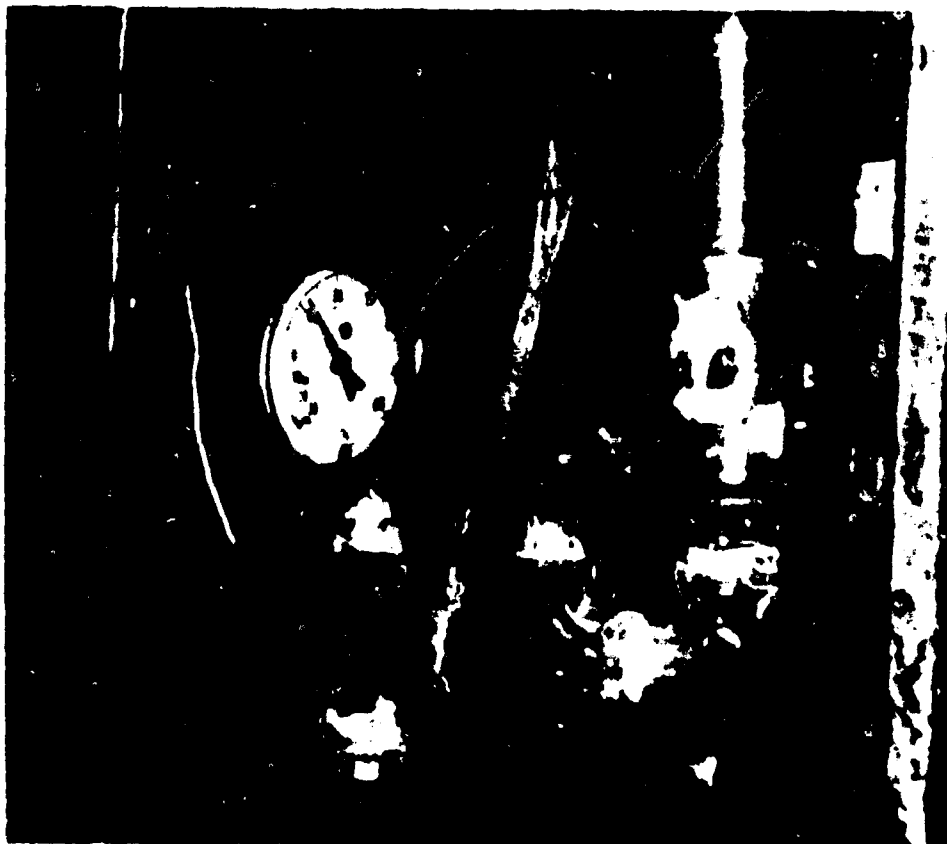
** Ambient temperature - 72 F

drain plumbing. Cask pressure was observed to be 13 psig, Figure A-2 on April 12, 1966. Cask water temperature was determined to be 86.8°F. There was no indication of increasing cask pressure in the several weeks that the cask remained sealed at the Battelle Hot Cell Laboratory.

As cask water samples were being taken, a high concentration of black scale was noted in the water initially drawn from the outlet. Table A-2 gives the calculated specific activities for the several radioisotopes found in the cask coolant. An X-ray spectrographic analysis of the black precipitate showed major constituents to be Fe, Cr, and Ni plus trace amounts of Cu, Zn, and Pb. No Eu was found.

Gas samples were taken from the cask void above the core and analysed using a mass spectrometer and 512 channel analyzer. Table A-3 shows the volume percent of various constituents present in four samples drawn from the gas outlet valve. Kr^{85} was the predominant radioactive isotope present in the gas sample investigated.

No damage to the PM-3A shipping package or associated hardware was detected. Figure A-3 shows three photographs of the shipping package. Figures A-3a and -b show photographs of the as-received shipping package; Figure A-3c shows a photograph of the bare shipping cask and skid.



TE00225

FIGURE A-2. PM-3A SHIPPING-CASK GAS PRESSURE,
APRIL 12, 1966



TE00197

a.



TE00195

b.



TE00204

c.

FIGURE A-3. GENERAL PHOTOGRAPHS SHOWING THE BATTELLE-RECEIVED CONDITION OF THE PM-3A SHIPPING PACKAGE AND CASK

TABLE A-2.

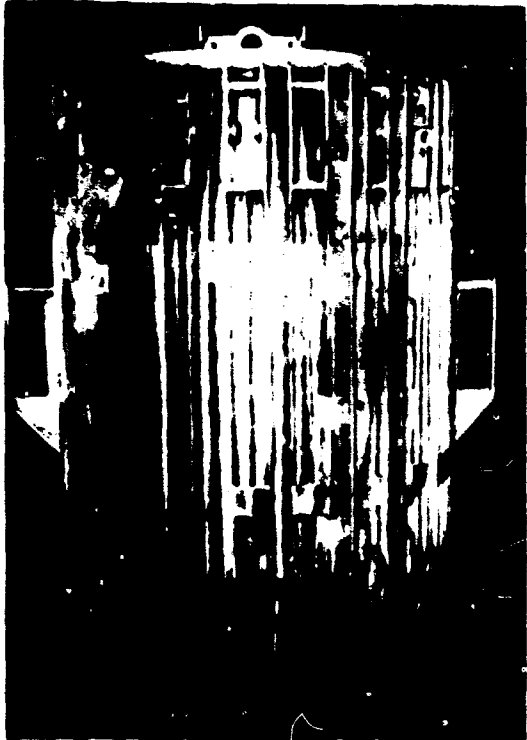
Isotope	Energy	Curies/cc
Co-60	1.17, 1.33	3.9×10^{-8}
Fe-59	0.20	2.1×10^{-8}
Te-127, Cs-137	0.68	5.7×10^{-7}
Mn-54, Co-58	0.83	1.1×10^{-7}
Y-91	1.21	5.4×10^{-8}

TABLE A-3. COMPOSITION OF GAS PRESENT IN CASK VOID ABOVE PM-3A CORE

Sample No.	Sample Volume, cc-atmospheres	Volume %				
		CO ₂	Ar	O ₂	N ₂	H ₂
1	4.58	3.83	0.58	3.23	47.8	44.5
2	4.21	3.80	0.58	3.29	47.9	44.4
3	3.60	2.52	0.59	4.00	49.3	43.6
4	3.72	2.34	0.60	4.10	49.5	43.5

Upon removing the cask from the Hot Cell storage pool and performing one cleaning with the steam cleaner, fission products adhering to the exterior surfaces of the cask resulted in 7000-11,000 counts per minute per 100 cm² of smearable activity. After alternate steam cleanings and hand rubdowns with Amway* paste cleaner, the smearable counts were reduced to 100 counts per minute per ¹⁰⁰cm². The entire outside surface of the cask was then sprayed with clear Krylon which reduced the smearable counts to background activity. Figure A-4 shows the bare shipping cask in the post-cleanup condition.

* Amway Corporation, Ada, Michigan.



TE00374

a.



TE00373

b.



TE00372

c.



TE00371

d.

FIGURE A-4 PHOTOGRAPHS SHOWING THE TMS-3A SHIPPING CASK AFTER UNLOADING AND PRIOR TO SHIPMENT FROM BATTEREE COLUMBUS

APPENDIX B

CORE HANDLING FIXTURE

The as-received core handling fixture could not be locked to the core shroud after being unlocked. In fact, the fixture cam could be rotated a full 360° with relatively little force. Inspection of the fixture indicated that the three stainless steel rods attached to the cam were bent to the point that the rod connecting pins had all disengaged from their slots within the cam. Consequently, the cam was free to rotate. Before the final closing of the shipping cask, the bent locking rods were removed from the core handling fixture, decontaminated, straightened, and placed back in their proper positions within the fixture. The fixture then operated properly.

Perhaps also worth noting here is the fact that one control rod hold-down screw, located on the core handling fixture, was frozen. Apparently the screw had frozen in a position that permitted ample distance to exist between the hold-down screw surface and the control rod pickup ball to allow proper seating of the fixture on the core shroud. The frozen hold-down screw was located opposite to the fixture unlocking pin. Since the fixture seemed to seat flush against the core shroud, no attempt was made to loosen the frozen screw.

UNCLASSIFIED

Security Classification

DOCUMENT CONTROL DATA - R&D		
<i>(Security classification of title, body of abstract and indexing annotation must be entered when the overall report is classified)</i>		
1. ORIGINATING ACTIVITY (Corporate author) Battelle Memorial Institute 505 King Avenue Columbus, Ohio		2a. REPORT SECURITY CLASSIFICATION UNCLASSIFIED
		2b. GROUP
3. REPORT TITLE POSTIRRADIATION EXAMINATION OF THE FM-3A TYPE 1 SERIAL 2 CORE PART 1. POSTIRRADIATION EXAMINATION OF FUEL TUBES		
4. DESCRIPTIVE NOTES (Type of report and inclusive dates) Interim Report		
5. AUTHOR(S) (Last name, first name, initial) John B. Brown Victor W. Storhok John E. Gates		
6. REPORT DATE 28 February 1967	7a. TOTAL NO. OF PAGES 82	7b. NO. OF REFS 17
8a. CONTRACT OR GRANT NO. NBy-63910	9a. ORIGINATOR'S REPORT NUMBER(S) None	
b. PROJECT NO.	9b. OTHER REPORT NO(S) (Any other numbers that may be assigned this report) None	
c.		
d.		
10. AVAILABILITY/LIMITATION NOTICES Distribution of this document is unlimited.		
11. SUPPLEMENTARY NOTES	12. SPONSORING MILITARY ACTIVITY Naval Facilities Engineering Command Washington, D. C. 20390	
13. ABSTRACT The FM-3A Type 1 Serial 2 core was removed from the reactor because of increasing fission product levels in the primary coolant. This increase in level was believed associated with defects in the 347 stainless steel fuel cladding. This examination was to locate defects and determine their cause. Cracks were found to penetrate the outer clad of the tubular elements in high-performance regions. All cracks were longitudinal and intergranular, generally starting at the outer tube surface and terminating at a fuel particle. No evidence of grain boundary precipitates or fuel matrix cracking was observed. On the basis of crack morphology and the similarity of the cracks to cracks attributed to stress-activated corrosion by other investigators, it was concluded that the most probable cause of clad cracking was a stress accelerated chemical attack of unknown origin.		

DD FORM 1473
1 JAN 64

UNCLASSIFIED

Security Classification

UNCLASSIFIED

Security Classification

14. KEY WORDS	LINK A		LINK B		LINK C	
	ROLE	WT	ROLE	WT	ROLE	WT
Reactor Core technology Cermet reactor fuel Reactor fuel failure Irradiation effects						

INSTRUCTIONS

1. **ORIGINATING ACTIVITY:** Enter the name and address of the contractor, subcontractor, grantee, Department of Defense activity or other organization (*corporate author*) issuing the report.
- 2a. **REPORT SECURITY CLASSIFICATION:** Enter the overall security classification of the report. Indicate whether "Restricted Data" is included. Marking is to be in accordance with appropriate security regulations.
- 2b. **GROUP:** Automatic downgrading is specified in DoD Directive 5200.10 and Armed Forces Industrial Manual. Enter the group number. Also, when applicable, show that optional markings have been used for Group 3 and Group 4 as authorized.
3. **REPORT TITLE:** Enter the complete report title in all capital letters. Titles in all cases should be unclassified. If a meaningful title cannot be selected without classification, show title classification in all capitals in parenthesis immediately following the title.
4. **DESCRIPTIVE NOTES:** If appropriate, enter the type of report, e.g., interim, progress, summary, annual, or final. Give the inclusive dates when a specific reporting period is covered.
5. **AUTHOR(S):** Enter the name(s) of author(s) as shown on or in the report. Enter last name, first name, middle initial. If military, show rank and branch of service. The name of the principal author is an absolute minimum requirement.
6. **REPORT DATE:** Enter the date of the report as day, month, year, or month, year. If more than one date appears on the report, use date of publication.
- 7a. **TOTAL NUMBER OF PAGES:** The total page count should follow normal pagination procedures, i.e., enter the number of pages containing information.
- 7b. **NUMBER OF REFERENCES:** Enter the total number of references cited in the report.
- 8a. **CONTRACT OR GRANT NUMBER:** If appropriate, enter the applicable number of the contract or grant under which the report was written.
- 8b, 8c, & 8d. **PROJECT NUMBER:** Enter the appropriate military department identification, such as project number, subproject number, system numbers, task number, etc.
- 9a. **ORIGINATOR'S REPORT NUMBER(S):** Enter the official report number by which the document will be identified and controlled by the originating activity. This number must be unique to this report.
- 9b. **OTHER REPORT NUMBER(S):** If the report has been assigned any other report numbers (*either by the originator or by the sponsor*), also enter this number(s).
10. **AVAILABILITY/LIMITATION NOTICES:** Enter any limitations on further dissemination of the report, other than those

imposed by security classification, using standard statements such as:

- (1) "Qualified requesters may obtain copies of this report from DDC."
- (2) "Foreign announcement and dissemination of this report by DDC is not authorized."
- (3) "U. S. Government agencies may obtain copies of this report directly from DDC. Other qualified DDC users shall request through _____."
- (4) "U. S. military agencies may obtain copies of this report directly from DDC. Other qualified users shall request through _____."
- (5) "All distribution of this report is controlled. Qualified DDC users shall request through _____."

If the report has been furnished to the Office of Technical Services, Department of Commerce, for sale to the public, indicate this fact and enter the price, if known.

11. **SUPPLEMENTARY NOTES:** Use for additional explanatory notes.
12. **SPONSORING MILITARY ACTIVITY:** Enter the name of the departmental project office or laboratory sponsoring (*paying for*) the research and development. Include address.
13. **ABSTRACT:** Enter an abstract giving a brief and factual summary of the document indicative of the report, even though it may also appear elsewhere in the body of the technical report. If additional space is required, a continuation sheet shall be attached.

It is highly desirable that the abstract of classified reports be unclassified. Each paragraph of the abstract shall end with an indication of the military security classification of the information in the paragraph, represented as (TS), (S), (C), or (U).

There is no limitation on the length of the abstract. However, the suggested length is from 150 to 225 words.

14. **KEY WORDS:** Key words are technically meaningful terms or short phrases that characterize a report and may be used as index entries for cataloging the report. Key words must be selected so that no security classification is required. Identifiers, such as equipment model designation, trade name, military project code name, geographic location, may be used as key words but will be followed by an indication of technical context. The assignment of links, roles, and weights is optional.

UNCLASSIFIED

Security Classification